Case study of a site-specific design and operation optimization of a wind farm co-located PEM electrolyzer and BESS including degradation

Dustin Frings[1], Georg Jacobs[1], Thorsten Reichartz[1], Thora Potthoff[1], Lucas Blickwedel[1], and Martin Knops[1]

[1]Chair for Wind Power Drives, RWTH Aachen University, Aachen, 52074, Germany

Correspondence to: Dustin Frings (dustin.frings@cwd.rwth-aachen.com)

Abstract. The expansion of volatile renewable energy sources leads to increased electricity price volatility and cannibalization effects, intensifying the economic pressure on project developers. Decentralized hybrid energy systems for renewable hydrogen production offer a solution to exploit these price fluctuations and counteract curtailment during hours of low or negative electricity prices. However, the design and operation of these systems are inherently coupled and significantly influenced by external factors, such as electricity and hydrogen prices that can be achieved over the lifetime. To determine an economically optimal design, specifically the power of an electrolyzer and the capacity of a battery, both site-specific and plant-specific characteristics must be considered.

First, this paper presents a methodology for determining the optimal electrolyzer rated power and lithium-ion buffer battery capacity for a 68 MW wind farm in north-western Germany. The approach extends an existing site-specific design method by introducing a battery energy storage system (BESS) and enhancing the electrolyzer model with part-load efficiency and operating-mode-dependent degradation. Results indicate that neglecting degradation leads to an underestimation of levelized cost of hydrogen (LCOH) by 1.2 € kg^{-1}, corresponding to 21 %, while neglecting both degradation and part-load efficiency increases this underestimation to 35 %. Concurrently, the inclusion of the BESS can reduce electrolyzer degradation by a fifth and increase the annual operational profit by 7 %, while the LCOH remains constant. For the design phase, a price-independent operational strategy aiming to maximize renewable hydrogen yield was implemented, representing a conservative operation simplification.

In a second step, this operational assumption within the design phase was compared to a mixed-integer linear (MIL) operational optimization. This assessment reveals two key findings: Firstly, the assumption of a constant achievable electricity price over the system's lifetime leads to a 23 % overestimation of annual operational profits when compared to the more realistic electricity sales on the German day-ahead market in 2024. Secondly, the operation heuristic of the design method demonstrates high economic competitiveness, deviating by only 2 %. However, reducing the hydrogen price considerably increases this deviation, highlighting the strong price-dependence of the operation strategy and demonstrating that the determined operation

assumptions within the design method significantly underestimate potential profits under altered price conditions. Nevertheless, this performance may be site-specific, as integrated optimization may yield significantly higher added value in markets characterized by greater price volatility or different meteorological profiles. Beyond these specific results, the model showcases the critical importance of integrating high-fidelity physical effects for electrolyzer models, alongside the strategic inclusion of battery storage. Furthermore, it demonstrates that a rigorous consideration of the operational strategy is necessary for a reliable system assessment to account for volatile external factors. Overall, the proposed method provides wind farm developers with a tool to evaluate and optimize site-specific wind-hydrogen-battery systems to derive strategic investment decisions.

1 Introduction

To achieve the European Union's climate target of reducing greenhouse gas emissions by 55 % by 2030 (European Parliament and Council, 2021), the share of renewable energy in the energy mix is planned to be increased to 42.5 % and the production of 10 million tons of green hydrogen is targeted by 2030 (European Commission 2026). However, the rapid expansion of renewable energies and their volatile electricity generation pose significant challenges for grid and wind farm (WF) operators, including curtailment and declining revenues from electricity sales. Besides grid-induced curtailments, cost-induced curtailment of WFs during hours of negative electricity prices reduces the utilization of available wind resources. Meanwhile, WF operators encounter revenue declines due to price cannibalization and high price volatility (Bechmann and Quick, 2025). Concurrently, the marginal cost of wind power production has already attained a relatively low level (Bošnjaković et al., 2022), with no further drastic cost reductions expected. These effects increase pressure on WF operators, forcing them to consider new revenue streams and operation concepts. One way to counter these problems is a hybrid power plants (HPP) consisting for example of a WF, a solar photovoltaic (PV) system, a battery energy storage system (BESS), and an electrolyzer to produce green hydrogen (Canbulat et al., 2021). The economic viability of such integrated systems is increasingly supported by the rapid decline in capital expenditures for key components. In particular, the cost of utility-scale BESS has decreased by over 80 % in the last decade (IRENA, 2024), enabling HPP configurations that were previously economically unfeasible. From an economic perspective, HPP can temporarily decouple renewable electricity generation from electricity sales, enabling a more efficient utilization of available wind resources, as wind power generation can continue during grid- or price-induced curtailment events. Additionally, HPP potentially offer ancillary services like secondary control reserve, voltage control, or black start capability (Robinius et al., 2017; van Phan et al., 2024; Cozzolino and Bella, 2024). From a business perspective, electricity generated during hours with low or negative electricity prices can be stored in BESS, sold later or converted into hydrogen. However, the additional flexibility in the operation of the HPP makes the operation and thus its optimal techno-economic design complex (Rozzi et al., 2025), as the operation moves beyond a simple wind-to-grid connection to encompass multiple, multi-directional power flows between the WF, the grid, the BESS, and the electrolyzer.

Various studies investigate the design of different types of HPP. Early assessments, such as by Schnuelle et al. (2020) and Fabianek and Madlener (2024), evaluated given system configurations without optimizing the underlying component capacities. Other recent optimization approaches lack detail by focusing exclusively on the main components, thereby neglecting the significant influence of site-specific conditions or balance-of-plant sub-systems such as hydrogen storage, pipelines, and compressors (Grant et al., 2024; Tezer, 2025). These aspects are considered within the design methodology introduced by Reichartz et al. (2024b), that minimizes the levelized cost of hydrogen (LCOH) for a WF-electrolyzer system. Giving the hourly WF power output over one year they optimize the electrolyzer design and the position of all components, including the point of water supply and different distribution modes like a hydrogen pipeline or storage combined with trailers. However, they used a highly simplified electrolyzer model with constant efficiency and without degradation effects. Yet, the operation of an electrolyzer strongly influences its degradation and therefore its efficiency loss (Papakonstantinou et al., 2020; Zheng et al., 2023; Sayed-Ahmed et al., 2024). Consequently, the proposed methodology underestimates maintenance and replacement costs and, therefore, the LCOH. Ibáñez-Rioja et al. (2025) minimize LCOH, model degradation, and component replacement for a WF, PV, water electrolyzer, hydrogen storage, and BESS. However, their case relies on assumptions regarding the demand side, specifically by assuming constant hydrogen demand and off-grid operation. Additionally, they used geological hydrogen storage that is highly location dependent. All the aforementioned studies on HPP design methodologies minimize LCOH, however, this keeps focus on reducing hydrogen system costs while maximizing the annual hydrogen product (AHP), although HPP operators aim to maximize the profit of the overall HPP. Accurately calculating this profitability requires an estimation of potential revenues, which in turn necessitates an approximation of the system's operation. To model this operation behavior of the systems components within the design stage a predefined operation strategies can be utilized, meaning it is initially defined at what time electricity is fed into an electrolyzer, a battery, or if considered the electricity grid (Hofrichter et al., 2023; Grant et al., 2024; Tezer, 2025). However, fixed operation strategies can lead to a suboptimal design compared to the actual system behavior under varying price conditions leading to potential over- or underestimated revenues and costs (Kansara and Roldán Serrano, 2024; Zheng et al., 2022). To overcome the issue of a predetermined operating strategy, two-stage optimization consisting of an outer design optimization and an inner operation optimization loop is utilized (Balderrama et al., 2019; Dolatabadi et al., 2019; Zheng et al., 2022; Shams et al., 2021). These approaches, however, ignore either part-load efficiency, degradation of the electrolyzer, or site-specific cost conditions. Moreover, some do not include a BESS, even though battery integration can enhance the HPP revenue potential and mitigate electrolyzer degradation (Peng et al., 2025; Nachit et al., 2026). While existing literature frequently investigates HPP design, many studies rely on simplified electrolyzer models or overlook site-specific infrastructure. Furthermore, the prevailing focus on LCOH minimization and fixed operating strategies often neglects the potential for profit maximization and the strategic synergies of battery integration in volatile market conditions. In this study, the observed HPP consists of a WF, a proton exchange membrane (PEM) electrolyzer, and a BESS as main components, as well as additional subcomponents consisting of a power cable, power converter, water pipe, water pump, hydrogen pipe, hydrogen compressor, and hydrogen storage.

To address the gaps in the existing literature, the distinct novelty of this work lies in the introduction of a comparative, two-step evaluation framework that quantifies the performance gap between heuristic design assumptions and optimized system operation. First, we establish a conservative baseline design. Following the approach of Hofrichter et al. (2023), the rated electrolyzer power and BESS capacity are sized to maximize the annual profit (AP) based on a fixed, rule-based operation strategy that defines power flows for all design components. Crucially, this initial design phase is coupled with a detailed degradation evaluation. In a second step, a mixed-integer linear (MIL) operation optimization is applied to this designed system to determine an idealized upper bound for operational revenues. This idealized MIL operation, which includes linearized part-load efficiency of the electrolyzer, is then subjected to an identical degradation evaluation, yielding a more realistic operational annual profit (OAP).

By contrasting these two approaches, we enable a direct comparison between the optimized, price-aware system operation and the conservative operation assumed during the initial design phase. Guided by this framework, this study investigates the optimized PEM electrolyzer rated power and BESS capacity for a given WF to maximize the annual profit under a fixed heuristic operating strategy. Furthermore, we evaluate how the integration of a BESS alongside dynamic operational constraints and degradation effects influences the LCOH. And finally, the study quantifies the exact extent to which the MIL operation optimization and the subsequent degradation evaluation can increase the OAP compared to the initial heuristic design phase.

To answer these questions, in Sect. 2 the methodology for the design optimization, the MIL operation optimization and the degradation evaluation with all underlying assumptions is described. Section 3 introduces a case study to which the methodology is applied and results are presented. In Sect. 4, results and limitations of the presented methodology are discussed and further research needs are indicated.

2 Methodology

The following section describes the fundamentals for understanding the extended design optimization (Sect. 2.2), that is based on the method of Reichartz et al. (2024a). The design method is extended by a more detailed electrolyzer model as described in Sect. 2.1 and the objective to maximize the AP instead of minimizing LCOH. A subsequent MIL operation optimization to evaluate the operation strategy assumed in the design optimization is described in Sect. 2.3. Figure 1 presents the overall methodology with all respective optimization and evaluation steps, inputs, parameters, optimization variables, and outputs.

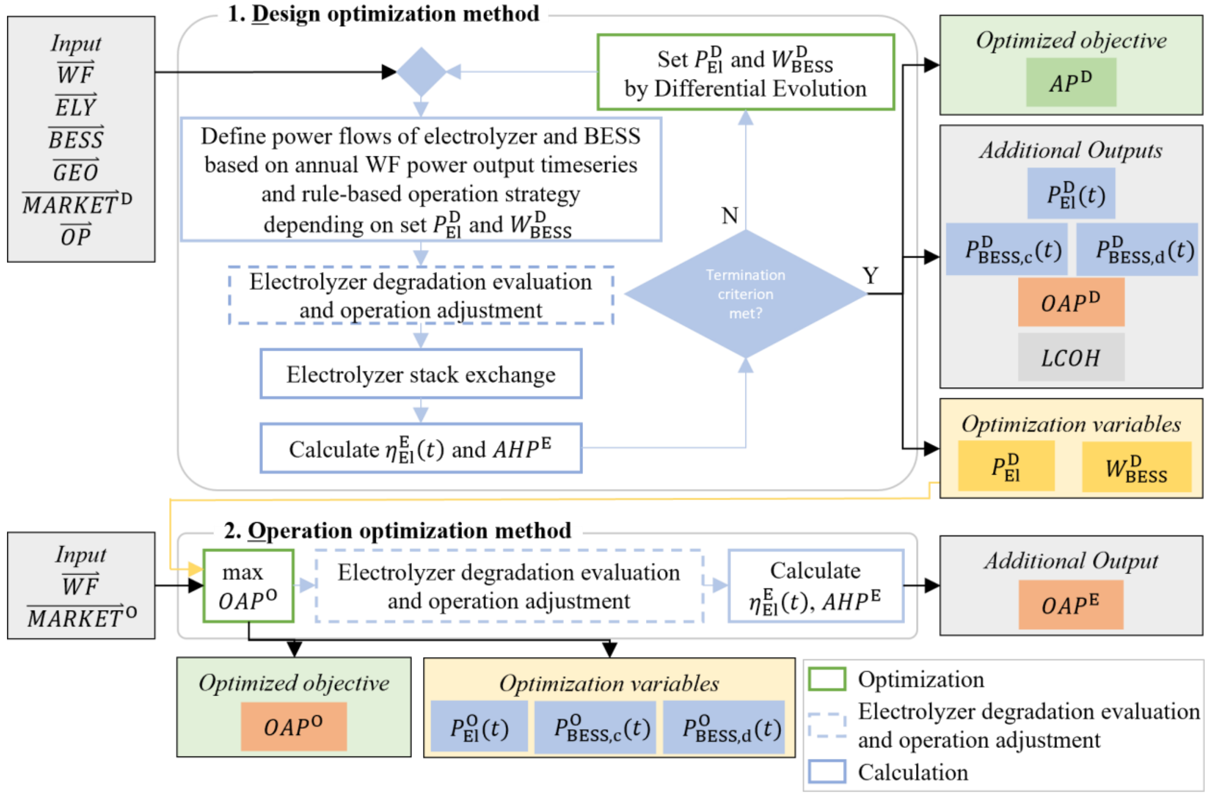

Figure 1: Schematic overview of the proposed design methodology (superscript index D) and the subsequent MIL operation optimization (superscript index O).

Before starting the design optimization input parameters need to be defined. The method described by Roscher (2020) is used to calculate the necessary WF input parameter vector $\overrightarrow{\boldsymbol{WF}}$. Based on an existing WF with a given nominal capacity P_{WF}, a site, weather data from the New European Wind Atlas (2026), the expected LCOE and a hourly time series of the WF power output $P_{\mathrm{WF}}(t)$ for a chosen weather year is calculated. The electrolyzer input parameter vector $\overrightarrow{\boldsymbol{EL}}$ depends on the electrolyzer technology and defines the permissible ranges for the electrolyzer rated power $P_{\mathrm{El}}^{\mathrm{D}}$ and BESS capacity $W_{\mathrm{BESS}}^{\mathrm{D}}$ within the components size is allowed to vary. It also contains the power ratio at which we assume the electrolyzer to operate in rated power mode $P_{\mathrm{El,rated}}^{\mathrm{min}}\ P_{\mathrm{El}}{}^{-1}$, the rated power P_{Stack} and the minimum part load $P_{\mathrm{Stack}}^{\mathrm{min}}$ of a single electrolyzer stack. Electrolyzer cell related parameters are the maximum current density $i_{\mathrm{cell}}^{\mathrm{max}}$, the maximum cell voltage $U_{\mathrm{cell}}^{\mathrm{max}}$, the cell area A_{cell}, the operating temperature T_{cell}, the operating pressure p_{H_2} and p_{O_2}, the transfer coefficients α_{H_2} and α_{O_2} and the exchange current densities i_{H_2} and i_{O_2} at cathode and anode. Finally, the electrolyzer input parameter vector contains the efficiency of the auxiliary electrolyzer components η_{Aux}, and the degradation rates $degR_{\mathrm{El},m}$ of each considered operation mode m which are defined in Sect. 2.2.2. Further input vector for the BESS $\overrightarrow{\boldsymbol{BESS}}$ consist of the roundtrip efficiency η_{BESS}, the $CRate$ as ratio between power and capacity, and the lifetime n_{BESS}. To take site specific conditions into account geodata is provided as vector $\overrightarrow{\boldsymbol{GEO}}$.

The shapefile sh_{El} determining the available area on which the electrolyzer can be placed, POCC the point of common coupling, $p_{\mathrm{H_2O}}$ the point of water access, p_{POD} the point of hydrogen demand. Besides these inputs, market data for the design optimization is given with the $\overrightarrow{\boldsymbol{MARKET}}^{\mathbf{D}}$ vector, assuming a constant hydrogen price $p_{\mathrm{H_2}}$ and a reference value (RV) describing the average expected electricity price achieved over the lifetime of the WF. For example in Germany the RV given by the Renewable Energy Sources Act (Federal Office of Justice, 2026) serves as good approximation. Market data for the operation optimization $\overrightarrow{\boldsymbol{MARKET}}^{\mathbf{O}}$ consist of an annual timeseries in hourly resolution of past day-ahead market prices instead of the RV. Finally, the observation period $\mathrm{ObservPeriod}$ as part of $\overrightarrow{\boldsymbol{OP}}$ is used to calculate the mean AHP.

The separation of the design phase and the MIL operation optimization serves to ensure a conservative long-term design and computational stability. Sizing a system for a 25-year lifetime faces profound uncertainties regarding spot market prices and wind profiles. Therefore, the design phase utilizes the year 2024, which represents, according to anemos (2024), an average wind and electricity yield year over the past 20 years and a constant reference value as electricity price. Relying on a predefined rule-based operation strategy during the design phase provides a conservative estimation of the system's operational revenues. Embedding a fully functional MILP model within every single iteration of the outer global search loop would increase the computational effort (Eltamaly and Almutairi, 2025) and introduce severe risks regarding numerical stability. If the inner solver experiences convergence issues in specific regions of the design space, the resulting numerical noise in the objective function would potentially disrupt the convergence behaviour of the outer optimization algorithm. Thus, the subsequent MIL operation optimization is applied exclusively to the finalized design to establish an idealized upper bound for revenues under actual volatile market conditions, allowing for a comparison against the conservative design assumptions.

Within the design optimization method, the design parameters P_{El} and W_{BESS} are iteratively adjusted by the Differential Evolution (DE) algorithm (Storn and Price, 1997), which is further described in Sect. 2.2.Within a single iteration, the operation of the electrolyzer and BESS is defined using a determined operation strategy as described in Sect. 2.2.1. Subsequently, the degradation of the electrolyzer is evaluated based on the previously determined operation according to the method detailed in Sect. 2.2.2. This evaluation framework recalculates the actual degradation-affected efficiency for each time step and structurally corrects the initial operational results to account for real-world performance losses. Based on the information regarding the degradation state of the electrolyzer stacks, the timing for stack replacement is decided as outlined in Sect. 2.2.3. Before the termination criterion for the DE optimization is verified, the electrolyzer efficiency is calculated for each time step as specified in Sect. 2.2.5. This calculation incorporates the cell voltage discussed in Sect. 2.1.1 and accounts for the actual degradation occurring as explained in Sect. 2.1.2. This process yields the AHP, the objective function value and the operational power data per time step for the electrolyzer $P_{\mathrm{EL}}(t)$ and for charging and discharging the battery. Additional results are the operation-dependent part of the annual profit (OAP), that consists of revenues from electricity and hydrogen sales, variable water procurement costs, and electrolyzer degradation costs. Finally, the LCOH and the optimal values of the design variables

P_{EL} and W_{BESS} are given as output. These optimized design variables serve as input for the operational optimization method described in Sect. 2.3, where the OAP^{O} is maximized through MIL optimization. To maintain mathematical linearity and ensure solver stability, this operation optimization step assumes a linearized part-load efficiency as calculated in Sect. 2.3.1 and tracks the electrolyzer degradation as detailed in Sect. 2.3.2 even though the impact of degradation on the electrolyzer efficiency is neglected. To address this limitation and guarantee a fair comparison with the design method, the optimized dispatch profile is subsequently subjected to the identical post-optimization degradation evaluation described above. This post-optimization step applies the degradation-dependent efficiency corrections to the optimized power flows, thereby penalizing the idealized hydrogen gains to report the true, realistic AHP^{E} and OAP^{E}.

2.1 Electrolyzer model

This work focuses on PEM technology for electrolyzers, as it offers a wider part-load range and rapid system response times compared to alternative methods. These characteristics make PEM technology superior for coupling with fluctuating renewable energy sources compared to other technologies such as alkaline electrolysis or solid oxide electrolysis (Bockelmann et al., 2024), which is why they are widely used in the literature for HPP. In the following sections the basics for calculating the polarization curve, degradation, and part-load efficiency of an electrolysis cell are presented.

2.1.1 Cell voltage

The load-dependent efficiency of a PEM electrolysis cell η_{cell} is calculated using the polarization curve as a function of the cell voltage U_{cell}. The polarization curve characterizes the electrochemical behavior of an electrolyzer cell and represents the relationship between the current density i_{cell} and the cell voltage U_{cell} (Buttler and Spliethoff 2018, 2440-54). i_{cell} refers to the current relative to the cell surface area A_{cell}. This paper uses an empirical model of an electrical equivalent circuit by Han et al. (2015) and Abdin et al. (2015), where U_{cell} equals the sum of the Nernst voltage U_{Nernst}, also called open circuit voltage, and the activation overpotential U_{act}, the ohmic loss overpotential U_{ohm}, and the diffusion overpotential U_{diff}, as seen in Eq. (1):

$$U_{\mathrm{cell}} = U_{\mathrm{Nernst}} + U_{\mathrm{act}} + U_{\mathrm{ohm}} + U_{\mathrm{diff}}. \tag{1}$$

The cell voltage under ideal conditions to operate the electrolysis is called the Nernst voltage. It is the theoretical minimum voltage for PEM electrolysis cells when other overpotentials are neglected and can be calculated using equation (2)-(4) (Han et al., 2015):

$$U_{\mathrm{Nernst}} = U_{\mathrm{rev}} + \frac{R \cdot T_{\mathrm{cell}}}{z \cdot F} \cdot \ln\left(\frac{a_{H_2} \cdot \sqrt{a_{O_2}}}{a_{H_2 0}} \right), \tag{2}$$

$$U_{rev} = 1.229 - 0.9 \cdot 10^{-3} (T_{cell} - 298\ K), \tag{3}$$

$$a_{H_2} = \frac{p_{\mathrm{H_2}}}{p_0}, a_{O_2} = \frac{p_{\mathrm{O_2}}}{p_0}, a_{\mathrm{H_2O}} = 1, \tag{4}$$

where U_{rev} is the reversible voltage under standard pressure conditions, R the gas constant, T_{cell} the electrolyzer operating temperature, z the number of electron moles participating at the electrolysis reaction, F the Faraday constant, $a_{\mathrm{H_2}}$ the ideal gas activity of hydrogen depending on the partial pressure $p_{\mathrm{H_2}}$ and the standard atmosphere pressure p_0, $a_{\mathrm{O_2}}$ the ideal gas activity of oxygen depending on the partial pressure $p_{\mathrm{O_2}}$, and $a_{\mathrm{H_2O}}$ the activity of liquid water. The activation overvoltage U_{act} derived from the Butler-Volmer equation (Carmo et al., 2013), must be applied to overcome the activation energy for the electrochemical reactions at the electrodes. Following Eq. (5) U_{act} is the sum of the cathode overpotential $U_{\mathrm{act,cat}}$ and the anode overpotential $U_{\mathrm{act,an}}$:

$$U_{\mathrm{act}} = U_{\mathrm{act,cat}} + U_{\mathrm{act,an}}, \tag{5}$$

with

$$U_{\mathrm{act,cat}} = \frac{R \cdot T_{\mathrm{cell}}}{\alpha_{\mathrm{cat}} \cdot F} \sinh^{-1}\left(\frac{i_{\mathrm{cell}}}{2 \cdot i_{o,\mathrm{cat}}}\right), \tag{6}$$

$$U_{\mathrm{act,an}} = \frac{R \cdot T_{\mathrm{cell}}}{\alpha_{an} \cdot F} \sinh^{-1}\left(\frac{i_{\mathrm{cell}}}{2 \cdot i_{o,\mathrm{an}}}\right), \tag{7}$$

where α_{cat} and α_{an} are the charge transfer coefficients and $i_{\mathrm{o,cat}}$ and $i_{\mathrm{o,an}}$ are the exchange current densities of the cathode respective the anode. U_{ohm} defines the ohmic overpotential caused by the electrolysis cell resistances. According to Ohm's law, it is calculated as the product of the electrical cell resistance R_{cell} and i_{cell}. The cell resistance consists mainly of the resistance of the cell membrane (Abdin et al., 2015), wherefore the resistance of the electrodes and bipolar plates are neglected. In this work, U_{ohm} is consequently represented as a function of i_{cell}, the membrane thickness δ_{m}, and the membrane conductivity σ_{m}, as seen in eq. (8).

$$U_{\mathrm{ohm}} = R_{\mathrm{cell}} \cdot A_{\mathrm{cell}} \cdot i_{\mathrm{cell}} = \frac{\delta_{\mathrm{m}}}{\sigma_{\mathrm{m}}} \cdot i_{\mathrm{cell}}, \tag{8}$$

where σ_m is a function of the membrane humidification degree λ and T_{cell}, following Eq. (9):

$$\text{with } \sigma_{\mathrm{m}} = (0.005139 \cdot \lambda - 0.00326) \cdot e^{1268 \cdot \left(\frac{1}{303} - \frac{1}{T_{\mathrm{cell}}}\right)}. \tag{9}$$

Finally, U_{diff} describes the diffusion overpotential caused by mass transport in the electrolyzer. Studies show that U_{diff} is much lower than U_{ohm} and U_{act} (Hernández-Gómez et al., 2020). For this reason, we follow other studies and assume U_{diff} to be zero (Görgün, 2006; Shiva Kumar and Himabindu, 2019; García-Valverde et al., 2012).

2.1.2 Degradation

Degradation can be understood as an additional voltage that must be overcome to enable electrolysis, adding an additional coefficient to Eq. (1). Factors influencing degradation include membrane and catalyst properties (Tomić et al., 2023; Buttler and Spliethoff, 2018), the operating temperature (Frensch et al., 2019), and the input power of the electrolyzer over time $P_{\mathrm{El}}(t)$. A comprehensive review on the influence and modeling approaches of degradation in PEM electrolyzer is provided by Makhsoos et al. (2025). Due to the high complexity of the different degradation mechanisms, we assume a fixed set of technical properties for the membrane, catalyst, temperature and pressure, while our focus in this work is the relationship between electrolyzer input power and its degradation. This aspect is of particular interest, as the electrolyzer is only powered by a WF, without any connection to the electricity grid. Tully et al. (2023) and so Lu et al. (2023) defining degradation rates for constant operation, fluctuating operation, and start-stop cycles of a PEM electrolyzer. Since the degradation rates from Tully et al. (2023) are experimentally validated, we assume these. We define a constant electrolyzer operation when the load difference for one hour of operation is lower than 3 % of the electrolyzers rated power P_{El}. If the load difference exceeds the limit the electrolyzer is assumed to operate fluctuating.

2.1.3 Efficiency

The efficiency of the electrolysis cell is modeled by considering the voltage efficiency and the Faraday efficiency. First, the Faraday efficiency η_F reflects losses due to gas diffusion and is defined as the ratio between the real hydrogen flow $\dot{n}_{\mathrm{H_2}}$ and the ideal hydrogen flow $\dot{n}_{\mathrm{H_2,ideal}}$, following Eq. (10):

$$\eta_F = \frac{\dot{n}_{\mathrm{H_2}}}{\dot{n}_{\mathrm{H_2,ideal}}}. \tag{10}$$

With the ideal hydrogen flow determined by Faraday's law based on the cell current density i_{cell}, the active cell area A_{cell}, the Faraday constant F, and the number of electrons transerred per hydrogen molecule formed z, calculated according to Eq. (11) (Yodwong et al., 2020):

$$\dot{n}_{\mathrm{H_2,ideal}} = \frac{i_{\mathrm{cell}} \cdot A_{\mathrm{cell}}}{z \cdot F}. \tag{11}$$

Second, the voltage efficiency η_V describes the ratio between the thermoneutral potential U_{th} and the actual cell voltage U_{cell} (Hernández-Gómez et al., 2020):

$$\eta_V = \frac{U_{\mathrm{th}}}{U_{\mathrm{cell}}} \tag{12}$$

The product of both efficiencies yields the cell efficiency η_{cell}, which relates the energy content of the produced hydrogen, based on the lower heating value $\Delta H_{\mathrm{H_2}}$ to the electrical input power, following Eq. (13):

$$\eta_{\mathrm{cell}} = \eta_V \cdot \eta_F = \frac{\Delta H_{\mathrm{H_2}} \cdot \dot{n}_{\mathrm{H_2}}}{U_{\mathrm{cell}} \cdot i_{\mathrm{cell}} \cdot A_{\mathrm{cell}}}. \tag{13}$$

Finally, equation (14) shows the overall efficiency of an electrolyzer η_{El} with multiple cells and stacks and can be calculated by η_{cell} and an additional efficiency for auxiliary structures η_{Aux} such as water and heat management systems (Cheng et al., 2025; Lu et al., 2023; Tofighi-Milani et al., 2025):

$$\eta_{\mathrm{El}} = \eta_{\mathrm{cell}} \cdot \eta_{\mathrm{Aux}} = \frac{\Delta H_{\mathrm{H_2}} \cdot \eta_F}{U_{\mathrm{cell}} \cdot z \cdot F} \cdot \eta_{\mathrm{Aux}}, \tag{14}$$

where η_{cell} is substituted to a combination of Eq. (10) and (13).

2.2 Design optimization

Within the design optimization the optimal rated power of the electrolyzer and the battery capacity are determined to maximize the overall profit over a defined observation period. This problem is formulated as a nonlinear optimization problem (NLP) with two continuous and non-negative decision variables, $P_{\mathrm{El}}^{\mathrm{D}}$ and $W_{\mathrm{BESS}}^{\mathrm{D}}$. It is solved using the DE algorithm. Due to its stochastic search strategy, this population-based approach enables a robust exploration of the complex design space while mitigating dependency on the initial starting point. Consequently, the best identified solution within the predefined termination criteria is reported as the optimal configuration. The search space for both the electrolyzer rated power and the BESS capacity is constrained between 0 and 30 % of the wind farm rated power based on the boundary insights from Chatzistlyianos et al. (2025) and Reichartz et al. (2024b). A random solver strategy was selected to maintain population diversity, utilizing a population factor of 15 and a crossover probability of recombination of 0.7 to balance vector mutation and target retention. To bypass local sub-optima and prevent population stagnation, dynamic scaling via dithering was applied with a mutation parameter of (0.5, 1). Computational execution was parallelized across all available CPU cores with the parameter workers set to minus one, which requires a synchronous population update scheme. Lastly, the optimization run was bounded by a maximum of 100 generations and a relative convergence tolerance of 0.001 to limit the computational overhead of the underlying hourly time-series optimization, while a fixed random seed of 1 ensures full numerical reproducibility of the optimization trajectories. The primary objective of design optimization is to maximize the AP of the HPP. The objective function is given in Eq. (15):

$$\max(\mathrm{AP}) = \max\big((\mathrm{AEP} - \mathrm{ECHS}) \cdot (\mathrm{RV} - \mathrm{LCOE}) + \mathrm{AHP} \cdot (p_{\mathrm{hy}} - \mathrm{LCOH})\big), \tag{15}$$

where AEP denotes the annual energy production of the WF and ECHS the total energy consumption of the hydrogen system (Reichartz et al., 2024b). The LCOE represents the average cost per unit of electricity generated by the WF over its lifetime, accounting for capital, operation, and maintenance costs. AHP is the annual hydrogen product that is delivered to the point of hydrogen demand and p_{hy} the assumed hydrogen price. Lastly, the LCOH are calculated according to Eq. (16):

$$\mathrm{LCOH} = \frac{\sum_c \left(\mathrm{CAPEX}_{y=0,c} + \mathrm{AF}_c \cdot \mathrm{OPEX}_c + \sum_{y=1}^{n} \frac{\mathrm{CAPEX}_{\mathrm{reinvest},c,y}}{(1+i)^y} - \frac{\mathrm{CAPEX}_{\mathrm{rest},c}}{(1+i)^n}\right)}{\sum_{y=1}^{n} \frac{M_{t,\mathrm{H_2}}}{(1+i)^y}}, \tag{16}$$

with the present value annuity factor AF_c following Eq. (17):

$$\mathrm{AF}_c = \frac{(1+i)^{n_c} - 1}{(1+i)^{n_c} \cdot i}. \tag{17}$$

The numerator of Eq. (16) represents the TOTEX of the hydrogen system and the denominator the discounted cumulative hydrogen production over the observation period n, where $M_{\mathrm{t,H_2}}$ denotes the hydrogen mass produced in year t. The parameter n_c specifies the lifetime of component c, and i the applied discount rate. The index c refers to the individual components of the hydrogen system consisting of the electrolyzer, battery, power cable, power converter, water and hydrogen pipeline, utilized water amount, and the hydrogen compressor and storage. Except for the battery these costs are calculated by the method of Reichartz et al. (2024a). $\mathrm{CAPEX}_{y=0,c}$ denotes the initial investment costs, while OPEX_c represents the annual operation and maintenance costs, which are annualized using AF_c. Reinvestment costs occurring in year y are given by $\mathrm{CAPEX}_{\mathrm{reinvest},c,y}$ and are discounted. The remaining value at the end of n is accounted by the residual cost term $\mathrm{CAPEX}_{\mathrm{rest},c}$.

2.2.1 Fixed operation strategy for electrolyzer and BESS

The operation of an electrolyzer and a BESS within a HPP influences the electrolyzers degradation and thus the amount of hydrogen produced. To overcome the complex HPP operation within the design method we define an operating strategy for the electrolyzer and BESS so that as much green hydrogen as possible gets produced. For the electrolyzer that means the strategy prioritizes supplying as much power as possible from the WF to the electrolyzer. This approach ensures a higher capacity factor of the electrolyzer increases hydrogen production and, at constant TOTEX, therefore reduces the LCOH. According to Equation (15), this would in turn lead to increased profit. Even though it is a strong simplification, is has been found to be a useful approach by Reichartz et al. (2024a). However, when modeling the electrolyzer's load-dependent efficiency and degradation, this conclusion is no longer straightforward, as TOTEX are not constant and hydrogen production is not strictly proportional to the input power. Nevertheless, this strategy is employed to obtain a reasonable solution. The battery is operated in a way that minimizes the number of shut-downs of the electrolyzer, thereby avoiding the high degradation associated with frequent start-stop cycles (Sect. 2.1.2).

The power flows in timestep t corresponding to the assumed operating strategy are shown in Figure 2 and described in the following section.

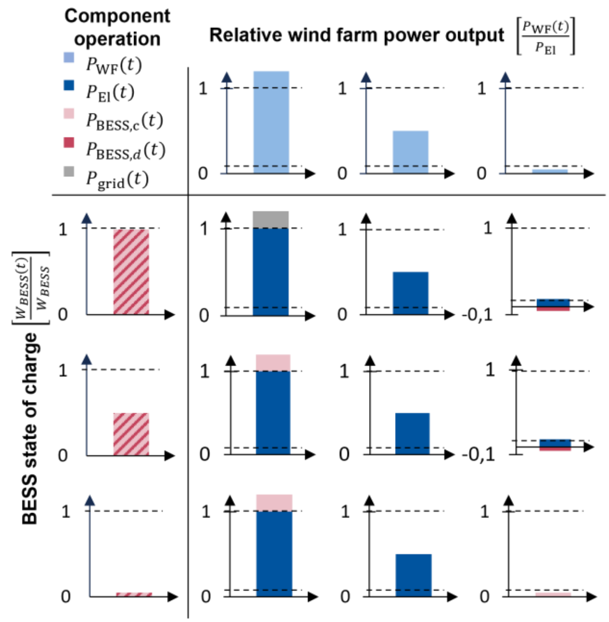

Figure 2: Power flows of HPP components for the determined operation strategy for a timestep depending on the relative WF power output (top row) and the BESS state of charge (left column).

The distribution of the WF power among the BESS, the electrolyzer, and the electricity grid, as defined in the assumed operating strategy, depends on both the WF power available at timestep t (top row, Figure 2) and the battery's state of charge at that timestep t (left column, Figure 2). If the available WF power exceeds the nominal power of the electrolyzer ($P_{\mathrm{WF}}(t)/P_{\mathrm{El}} > 1$), the electrolyzer operates at rated power. Any surplus power is used to charge the BESS. If the BESS is already fully charged, the excess power is fed into the grid. If the WF power is below the nominal electrolyzer power but above the minimum operating threshold ($P_{\mathrm{El}}^{\mathrm{min}}$), the entire wind farm power is supplied to the electrolyzer. In the final case, the wind power is insufficient to meet the minimum part-load requirement of the electrolyzer. If the battery has sufficient state of charge to compensate for the deficit relative to the electrolyzers minimum load ($W_{\mathrm{BESS}}(t) \geq P_{\mathrm{El}}^{\mathrm{min}} - P_{\mathrm{WF}}(t)$), it is discharged accordingly, thereby preventing a shutdown of the electrolyzer. If that is not the case, the electrolyzer must be shut down. The remaining wind power is then used to charge the battery.

2.2.2 Electrolyzer degradation evaluation

In the literature, degradation studies primarily investigate constant and fluctuating electrolyzer input power as well as start–stop operation (Sect. 2.1.2). Some studies distinguish between steady-state operation at full load, part load and off state. Based on this, the following operating states are defined within our model:

1. Steady-state operation at rated power (rated)
2. Steady-state operation at part-load (partl)
3. Steady-state operation at off-state (off)

4. Fluctuating operation (fluct)
5. Start-stop operation (stop)

Since no universal definitions of these operating states exist, a formal definition of a steady-state operation was introduced in Sect. 2.1.2. Figure 3 shows a flowchart of the degradation evaluation process. For the evaluation of degradation up to timestep t, binary decision variables $b_m(t)$ are introduced for each defined operating mode $m \in \{\text{rated}, \text{partl}, \text{off}, \text{fluct}, \text{stop}\}$. These variables are multiplied by the corresponding degradation rates $degR_{\text{El},m}$ to calculate the cumulative degradation $Deg_{\text{El}}(t)$ until t. The degradation associated with a start-stop cycle is added at the time of shutdown.

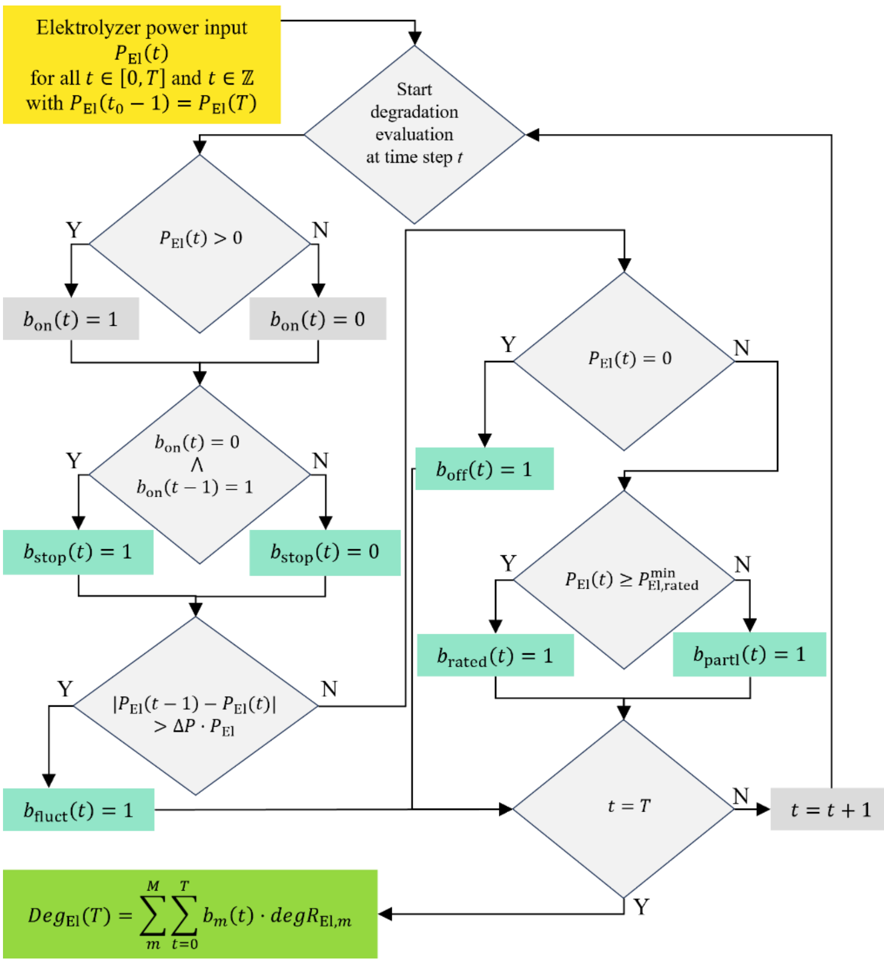

Figure 3: Flowchart to evaluate the operation dependent degradation of an electrolyzer.

Giving the electrolyzers input power $P_{\text{El}}(t)$ for each time step, the degradation evaluation loop starts with t equals zero and iteratively increases until t equals T. First, an auxiliary variable $b_{\text{on}}(t)$ is introduced to indicate whether the electrolyzer is operating at time t ($b_{\text{on}}(t) = 1$) or not ($b_{\text{on}}(t) = 0$). Subsequently, it is checked whether the electrolyzer has been switched off at time t, which corresponds to a transition from the on-state at the previous time step t-1 ($b_{\text{on}}(t-1) = 1$) to the off-state in t ($b_{\mathrm{on}}(t) = 0$). Next, based on the previously defined definition for steady-state operation, it is decided whether the electrolyzer is operating in steady state or fluctuating mode. If the input power is classified as steady, the absolute value of the input power is used to distinguish between constant off-state ($b_{\mathrm{off}}(t) = 1,\ if\ \ P_{\mathrm{El}}(t) = 0$), constant full-load operation ($b_{\mathrm{rated}}(t) = 1,\ if\ \ P_{\mathrm{El}}(t) > P_{\mathrm{El,rated}}^{\mathrm{min}}$) and constant part-load operation (($b_{\mathrm{partl}}(t) = 1$, otherwise). The operating modes fluct, off, rated, and partl are mutually exclusive. Accordingly, if one binary variable equals one at t, all others are equal to zero at that time. Using this method, the operation-dependent degradation over the entire year can be determined by multiplying the binary variables for each operating mode and timestep with the corresponding degradation rates.

2.2.3 Electrolyzer stack exchange

The degradation of the electrolyzer stacks might result in a need for replacement over their lifetime. Within the model, a stack replacement resets the degradation state to zero, incurring replacement costs. Other modeling approaches commonly assumed a fixed stack lifetime (Lim et al., 2021) or a replacement criterion based on a predefined efficiency loss of approximately 10 % (Grant et al., 2024; Ibáñez-Rioja et al., 2025). In this study, an alternative and more physically grounded approach is adopted. According to Buttler and Spliethoff (2018) the cell voltage of PEM electrolyzers ranges between 1.65 V and 2.5 V at a nominal current density of 2 A cm^{-2}, which directly maps to lower heating value efficiencies between 76 % and 50 %, respectively. In this study, the initial cell voltage at the beginning of life (BOL) is calculated via the polarization curve model (Sect. 2.1.1) as $U_{cell}^{\mathrm{BOL}} = 1.93$ V, corresponding to $\eta_{\mathrm{cell}}^{\mathrm{BOL}} = 0.64$. Due to degradation-induced overvoltages, the required cell voltage to maintain nominal current increases over time. The stack replacement threshold is set to a maximum limit of 2.5 V, representing an end-of-life criterion where cell efficiency drops to the literature-reported minimum of 50 %.

Stack replacement is restricted at the end of a year and all stacks within the electrolyzer are operated in the same way. During the optimization of P_{El} and W_{BESS}, the latest technically permissible replacement time is selected. The time of a stack replacement decision $X_{s,y}$ is formulated as a binary decision variable and a constraint is imposed to ensure that the maximum allowable cell voltage is not exceeded. The binary decision variable $X_{s,y}$ is therefore defined for each stack s and indicates whether the stack is replaced at the end of year *y* or not, following Eq. (18):

$$\mathrm{X_{s,y}} = \begin{cases} 1 & \text{replacement of stack s in } y \\ 0 & \text{otherwise} \end{cases} \quad \forall\ s \in Stacks\ , y \in ObservPeriod. \tag{18}$$

The costs for stack replacements $CAPEX_{SE,y}$ in year y are modeled according to Eq. (19):

$$CAPEX_{SE,y} = \sum_{s=1}^{S} \frac{z_{Stacks} \cdot CAPEX_{El}}{S} \cdot X_{s,y} \tag{19}$$

The parameter z_{Stacks} denotes the share of stack costs relative to the total electrolyzer investment costs $CAPEX_{El}$. According to the International Renewable Energy Agency (IRENA), approximately 45 % of the total system costs are attributed to the stacks, while 55 % relate to balance-of-plant components (IRENA, 2020). In general, significant future cost reductions are expected for PEM electrolyzer stacks due to their high cost-reduction potential (Smolinka et al., 2018). For this reason, a reduced cost share of $z_{Stacks} = 40$ % is assumed. $CAPEX_{El}$ describes the specific investment costs of PEM electrolyzers, which are assumed to be 1000 € kW^{-1}. Dividing this value by the number of stacks S that constitute the electrolyzer allows the investment cost of a single stack to be determined. Both the costs of all stack replacements and the resulting reduction in cumulative degradation are accounted for the computation of the AP.

2.2.4 Electrolyzer efficiency and annual hydrogen production

All calculations and formulations required to determine efficiency and degradation have been presented in the previous sections. These elements are consolidated in the following in order to compute the AP. The efficiency of the electrolyzer is calculated based on Equation (14) in Sect. 2.1.3 . In addition to physical constants, the efficiency depends on the cell voltage $U_{cell}(t)$ and the Faraday efficiency $\eta_F(t)$. The cell voltage is linked to the current density i_{cell}, and thus to the electrolyzer input power, through the polarization curve. Furthermore, $U_{cell}(t)$ increases over time due to degradation. The cumulative degradation up to timestep t was described in Sect. 2.2.2. Consequently, the cell voltage is expressed as

$$U_{cell}(t) = f_{polarisation\_curve}(i_{cell}(t)) + Deg_{El}(t). \quad (20)$$

In the case of a stack replacement, the cumulative degradation is reset to zero; otherwise, it increases continuously over the operating period. In addition to the cell voltage, the Faraday efficiency must be determined to calculate the overall efficiency. It is computed according to the model proposed by Yodwong et al. (2020):

$$\eta_F = \left(-0.0034 \cdot p_{H_2} - 0.001711\right) \cdot \frac{A_{cell}}{i_{cell}} + 1 \quad (21)$$

where p_{H_2} represents the operating pressure at the cathode of the PEM electrolyzer. This allows the electrolyzer efficiency to be fully determined for each timestep. With this the AHP is obtained by multiplying the electrolyzer input power at each t by the corresponding efficiency and summing over the entire year:

$$AHP = \sum_{t=0}^{8760} P_{El}(t) \cdot \eta_{El}(t) \quad (22)$$

With the AHP, finally, all parameters and variables of Eq. (15) are determined. In the following section a method is presented to verify the assumed operation strategy for the electrolyzer and BESS within the design optimization. This is done by a supplementary MIL operation optimization model using the previous optimized design variables P_{El}^D and W_{BESS}^D as fixed input parameters.

2.3 Operation optimization

This subsection introduces the MIL operation optimization of the HPP system over one year with hourly resolution, implemented in the Open Energy Modelling Framework (oemof) (Hilpert et al., 2018; Krien et al., 2020), which we further expanded. As shown in Figure 1 the aim is to maximize the OAP of the previous designed P_{El} and W_{BESS} through optimizing the operation of the electrolyzer and BESS under time-varying electricity prices and WF power generation. Within the operation optimization the electrolyzer part-load efficiency curve calculated based on Sect. 2.2.4 gets linearized according to Sect. 2.3.1. The operation-dependent degradation of the electrolyzer is calculated within the operation optimization following Sect. 2.3.2, but its influence on the efficiency cannot be incorporated since it would introduce non-linearities. Therefore, the actual efficiency losses associated with degradation are neglected during the MIL operation optimization. After the optimization, however, an evaluation following the procedure described in Sect. 2.2.2 is conducted to determine the real degradation, with which the actual electrolyzer efficiency $\eta_{El}^{O}(t)$ at each timestep and the annual hydrogen production AHP^{O} can be calculated. Additionally, for the BESS, linear cycle-based degradation costs are added to the objective function that is defined as

$$\max(\mathrm{OAP}) = \max(\sum_{t=0}^{T}\left(SE(t) \cdot p_{\mathrm{elec}}(t) + SH(t) \cdot p_{\mathrm{hy}}(t) - WSC(t)\right) - DegC_{\mathrm{El}} - DegC_{\mathrm{BESS}}), \quad (23)$$

where $SE(t)$ denotes the electricity sold to the day-ahead market at each timestep t, remunerated at the corresponding market price $p_{\mathrm{elec}}(t)$. $SH(t)$ represents the amount of hydrogen sold, valued at the assumed hydrogen price $p_{\mathrm{H_2}}$. $WSC(t)$ accounts for the time-dependent water supply costs associated with hydrogen production and the term $\mathrm{DegC_{El}}$ represents the electrolyzer degradation costs and is calculated as

$$\mathrm{DegC_{El}} = \frac{TAD}{U_{cell}^{max} - U_{cell}^{t_0}(\mathrm{i}_{cell}^{max})} \cdot CAPEX_{SE}, \quad (24)$$

where TAD denotes the total annual degradation of the electrolyzer. $U_{\mathrm{cell}}^{\mathrm{max}}$ is the maximum allowable cell voltage, while $U_{\mathrm{cell}}^{t_0}(\mathrm{i}_{\mathrm{cell}}^{\mathrm{max}})$ denotes the cell voltage at nominal current $\mathrm{i}_{\mathrm{cell}}^{\mathrm{max}}$ at the beginning of operation t_0. The parameter $CAPEX_{SE}$ represents the stack exchange costs according to Eq. (19). $\mathrm{DegC_{BESS}}$ denotes the degradation costs of the BESS, defined as

$$\mathrm{DegC_{BESS}} = \mathrm{DegC_{BESS,specific}} \cdot \Delta t \cdot \sum_{t=0}^{T}(P_{\mathrm{BESS,c}}(t) + P_{\mathrm{BESS,d}}(t)), \quad (25)$$

where $\mathrm{DegC_{BESS,specific}}$ represents the specific BESS degradation costs. These costs are calculated as a function of the maximum number of cycles until the end of life $\mathrm{n_{cycles}}$, the depth of discharge DoD, and the roundtrip efficiency η_{BESS}, according to Eq. (26):

$$\mathrm{DegC_{BESS,specific}} = \frac{CAPEX_{\mathrm{BESS,specific}}}{n_{\mathrm{cycles}} \cdot 2 \cdot DoD \cdot \eta_{\mathrm{BESS}}}. \quad (26)$$

The OAP monetizes electricity and hydrogen revenues while internalizing water supply and degradation costs of the electrolyzer and BESS, thereby incentivizing profit-maximizing operation that accounts for both immediate market returns and long-term capital preservation.

2.3.1 Linearization of electrolyzer part load efficiency

The part-load efficiency of the electrolyzer can be calculated according to Sect. 2.2.4 and is linearized within the operation optimization. An example of a non-linear and a linearized electrolyzer part-load efficiency and power output over the power input is shown in Figure 4.

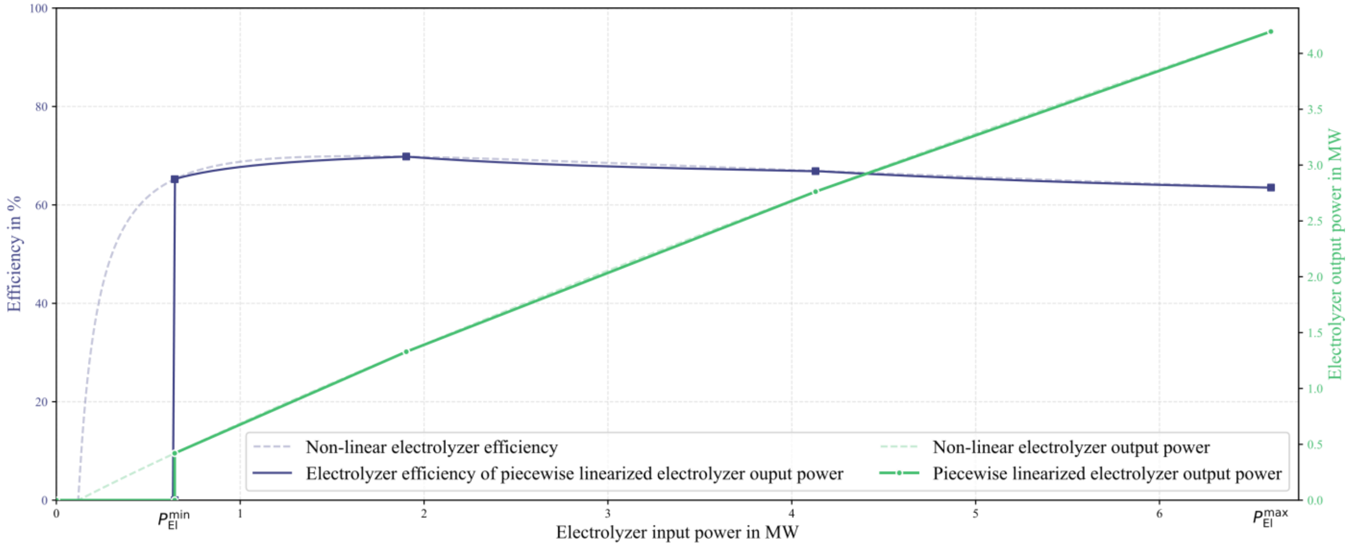

Figure 4: Exemplary illustration of the non-linear and piecewise linearized part-load electrolyzer power output (right axis) and the non-linear part-load efficiency and the efficiency of the linearized output power of an electrolyzer (left axis) in relation to the electrolyzer input power.

Figure 4 illustrates the linearization of the electrolyzer model used in the optimization framework. The primary y-axis (right) depicts the output power as a function of the electrolyzer input power. To accurately represent operational constraints, the model accounts for a minimum load threshold $P_{\mathrm{El}}^{\mathrm{min}}$. Below this point, the system remains in standby mode with zero output, followed by a vertical discontinuity at to reach the physical operating curve. The green segments represent the piecewise linearization, showing a high degree of fit with the non-linear physical reference (dashed green). The secondary y-axis (left) shows the corresponding electrolyzer efficiency. A key feature of this visualization is the actual piecewise efficiency (solid purple line). Unlike a direct linearization of efficiency, this curve is derived from the linearized power segments (dashed green). This results in a hyperbolic efficiency progression within each linear segment, highlighting the model's ability to capture the characteristic part-load efficiency increase while maintaining the linearity required for ML programming. The discrepancy between the solid and dashed purple lines quantifies the approximation error introduced by the choice of breakpoints. The piecewise linearized part-load input-output relation of the electrolyzer power was implemented in oemof according to Gurobi Optimization (2026).

2.3.2 MIL electrolyzer degradation model

In order to take the operation-dependent degradation of the electrolyzer within the operation optimization into account, the following constraints are integrated into oemof. The TAD is equal to the sum of the annual degradation AD_m of the degradation mode m, as seen in Eq. (25).

$$TAD = \sum_m^M AD_m \tag{25}$$

The same five degradation modes as shown in Sect. 2.2.2 are considered. Following Eq. (26) AD_m is calculated as the sum over all timesteps t until T of the binary variable $b_m(t)$ indicating if m is active at t or inactive, multiplied with its degradation rate $degR_{El,m}$.

$$AD_m = degR_{El,m} \cdot \sum_{t=0}^{T} b_m(t) \quad (26)$$

With Eq. (27) it is ensured that exactly one of each constant modes is active at t:

$$b_{off}(t) + b_{partl}(t) + b_{rated}(t) = 1 \quad (27)$$

Further Eqs. (28) – (32) are needed to determine whether the electrolyzer operates in constant partial load state or at rated power. Therefore, the auxiliary power variables for constant partial load $I_{partl}(t)$ and for constant rated power $I_{rated}(t)$ are introduced. As shown in Eq. (28) the sum of these auxiliary power variables is equal to the electrolyzer input power $P_{El}(t)$:

$$P_{El}(t) = I_{partl}(t) + I_{rated}(t). \quad (28)$$

Equation (29) to (32) identifying at which electrolyzer input power range the constant part-load or the constant rated power mode is active:

$$I_{partl}(t) \geq b_{partl}(t) \cdot P_{El}^{min}, \quad (29)$$

$$I_{partl}(t) \leq b_{partl}(t) \cdot 0.95 * P_{El}, \quad (30)$$

$$I_{rated}(t) \geq b_{rated}(t) \cdot (0.95 * P_{El} + \varepsilon), \quad (31)$$

$$I_{rated}(t) \leq b_{rated}(t) \cdot P_{El}. \quad (32)$$

To prevent equation (30) and (31) both being satisfied at 95 % P_{El}, an ε is introduced that clearly separates the two modes from each other. Besides the constant operation modes, the electrolyzer can be in fluctuation mode if active. To describe this mode the auxiliary variable $ALD(t)$ is needed as the absolute value of the electrolyzer input power difference between two consecutive timestep. As expressed in Eq. (33) $ALD(t)$ is the sum of the positive load difference $PLD(t)$ and the negative load difference $NLD(t)$:

$$ALD(t) = PLD(t) + NLD(t), \quad (33)$$

whereas $PLD(t)$ and $NLD(t)$ denote the positive and negative components of the load difference. Their definition depends on the rated electrolyzer power P_{El} and the binary variable pos, as expressed in Eq. (34) and (35):

$$PLD(t) \leq P_{El} \cdot pos, \quad (34)$$

$$NLD(t) \leq P_{El} \cdot (1 - pos). \quad (35)$$

pos indicates the sign of the load difference $LD(t)$ and results from subtracting the electrolyzer input power at the previous timestep t-1 from that at timestep t according to Eq. (36), allowing further decomposition into its positive $LD(t)$ and negative parts $NLD(t)$ following Eq. (37):

$$LD(t) = P_{El}(t) - P_{El}(t-1), \tag{36}$$

$$LD(t) = PLD(t) - NLD(t). \tag{37}$$

To determine when the fluctuating mode and therefore the binary variable $b_{fluct}(t)$ is active, $ALD(t)$ is linked to a minimum power threshold ΔP_{El}^{min}, as seen in Eqs. (38) and (39). This ensures that only sufficiently large changes in input power are classified as fluctuations.

$$ALD(t) \geq b_{fluct}(t) \cdot \Delta P_{El}^{min} \tag{38}$$

$$ALD(t) \leq b_{fluct}(t) \cdot P_{El} + \Delta P_{El}^{min} \tag{39}$$

The stop mode is governed by constraints expressed in Eqs. (40) – (41), which ensure that transitions to the turned-off state are correctly detected and represented within the model:

$$b_{stop}(t) \geq b_{off}(t) - b_{off}(t-1) \ , \tag{40}$$

$$b_{stop}(t) \leq b_{off}(t-1), \tag{41}$$

$$b_{stop}(t) \leq 1 - b_{off}(t), \tag{42}$$

where the binary variable $b_{stop}(t)$ can be described by equations that only depend on the constant off binary variable at different timesteps. At each timestep, it must be guaranteed that the electrolyzer operates either in a constant or a fluctuating mode; this coupling of corresponding binary variables is established using Eqs. (43) and (44).

$$b_{fluct}(t) + b_{const.}(t) = 1 \tag{43}$$

$$b_{off,c}(t) + b_{partl,c}(t) + b_{rated,c}(t) = b_{const}(t) \tag{44}$$

Distinguishing among constant operating modes requires additional auxiliary variables, introduced as shown in Eqs. (45) - (47), to ensure an unambiguous assignment to each respective state.

$$b_{partl,c}(t) \leq b_{partl}(t) \tag{45}$$

$$b_{partl,c}(t) \leq b_{const}(t) \tag{46}$$

$$b_{partl,c}(t) \geq b_{partl}(t) + b_{const}(t) - 1 \tag{47}$$

Finally, further constraints given in Eqs. (48) - (50) ensure correct identification of operation at rated power within the set of constant modes.

$$b_{rated,c}(t) \leq b_{rated}(t) \tag{48}$$

$$b_{rated,c}(t) \leq b_{const}(t) \tag{49}$$

$$b_{rated,c}(t) \geq b_{rated}(t) + b_{const}(t) - 1 \tag{50}$$

3 Model application and results

In this section the methodology outlined in Sect. 2 is applied to a case study of an existing WF in Germany. The use case and the assumed input parameters are defined in Sect. 3.1. Section 3.2 presents the results of the design optimization for maximizing the AP of the HPP and the influence of the added electrolyzer model and a BESS. Finally, Sect. 3.3 provides a comparative analysis between the operating strategy of the design optimization and the results of the operation optimization described in Sect. 2.3 and the subsequent degradation evaluation of Sect. 2.2.2.

3.1 Use case

The existing WF “Rhede (Ems)” with 21 turbines and a rated power of 67.55 MW (Windpark Rhede GmbH & Co. KG, 2025), located in North-West of Germany is considered. The WF area, the distance to the point of common coupling, the water supply point, the location of the electrolyzer, a part of the planed German hydrogen grid (Federal Network Agency, 2026), and the assumed wind rose taken from the New European Wind Atlas (2026) at the center of the wind farm site at 100 m height above the ground level are shown in Figure 5.

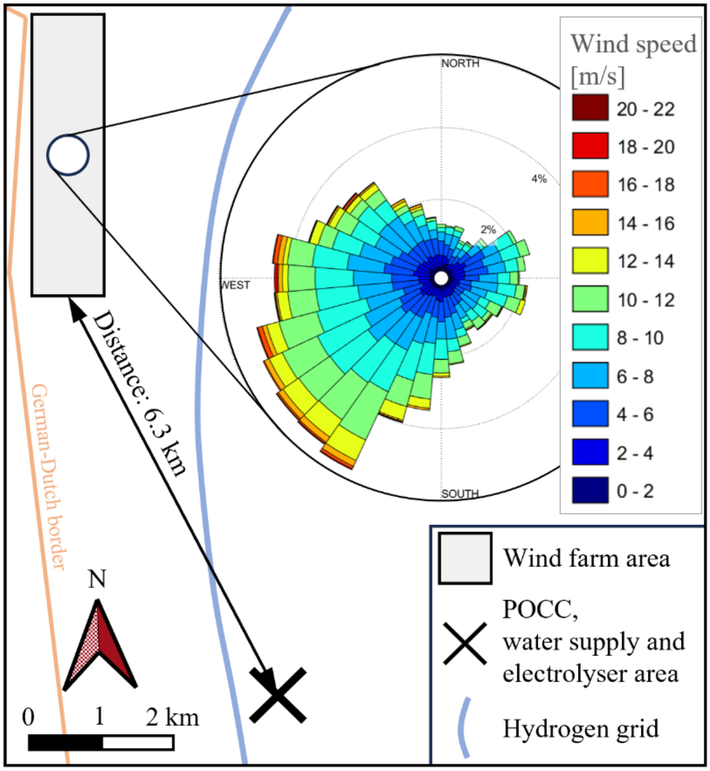

Figure 5: Schematic illustration of the wind farm site and its distance to the POCC, the water supply and the location of the electrolyzer. Also shown is a part of the planned German hydrogen grid and the wind rose at the center of the wind farm site at 100 m height above ground level.

The closest distance between the assumed hydrogen grid and the location of the electrolyzer is 0.61 km. Additionally a factor to transfer the direct distance to a more realistic distance of 1.4 is assumed (Reuß, 2019). Since focus of this work are the systems components and their model and operation we do not consider multiple distribution modes. Consequently, we assume that produced hydrogen will be compressed and delivered to the hydrogen grid via pipeline, where the hydrogen grid is modeled as an infinite sink. For a more detailed understanding of the distribution options, the subcomponents available in the model, and the cost functions assumed in this work, please refer to Reichartz et al. (2024a). For the BESS we assume a lifetime of 10 years (Lynus, 2026), CAPEX of 612 \$ $\mathbf{kWh^{-1}}$ according to Cole et al. (2025) with an exchange rate for 2024 of 0.92 € $\$^{-1}$ (OECD Economic Surveys: European Union and Euro Area 2025, 2025) to 560 € kWh^{-1}, and OPEX of 1 % CAPEX per year. Assumed technical design optimization parameters for the input vectors of Figure 1 are listed in Table 1 with their corresponding values and sources.

Table 1: Input vectors with assumed parameters for the design optimization.

Vector	Parameter	Value	Unit	Source
$\overrightarrow{WF}$	Levelized Cost Of Electricity: LCOE	55.2	€ MWh^{-1}	Own calculations based on Roscher (2020)
	Wind farm power output: $P_{\text{WF}}(t)$	Time series	MW	
$\overrightarrow{EL}$	Minimum rated power: $P_{\text{El,rated}}^{\text{min}}$	0.95 P_{El}	-	-
	Rated stack power: P_{Stack}	1.25	MW	Nel (2025), Bosch (2025)
	Minimum relative partial load: $P_{\text{Stack}}^{\text{min}}$	0.10 P_{Stack}	-	
	Maximum current density: $i_{\text{cell}}^{\text{max}}$	2	A cm^{-2}	Buttler and Spliethoff (2018)
	Maximum cell voltage: $U_{\text{cell}}^{\text{max}}$	2.5	V	
	Cell area: A_{cell}	0.095	m²	
	Operating temperature: t_{El}	80	°C	Han et al. (2015)
	Operating pressure cathode: p_{H_2}	13.78	bar	
	Operating pressure anode: p_{O_2}	1.013	bar	
	Transfer coefficient cathode: α_{H_2}	0.5	-	
	Transfer coefficient anode: α_{O_2}	2.0	-	
	Exchange current density cathod: i_{H_2}	0.1	A cm^{-2}	Abdin et al. (2015)
	Exchange current density anode: i_{O_2}	10^{-7}	A cm^{-2}	
	Efficiency of subcomponents: η_{Aux}	0.90	-	Cheng et al. (2025)
	Degradation rates for each operation mode: $degR_{\text{El},m}$	rated: 3 partl: 3 off: 3 fluct: 23.9 stop: 237	μV h^{-1}	Tully et al. (2023)
$\overrightarrow{BESS}$	Roundtrip efficiency: η_{BESS}	0.90	-	Kurzweil and Dietlmeier (2018)
	Lifetime T_{BESS}	10	years	-
	Specific CAPEX $CAPEX_{\text{BESS,specific}}$	560	€ kWh^{-1}	Cole et al. (2025)
	C-rate: CRate	1	h^{-1}	-
$\overrightarrow{GEO}$	Shapefiles and points determining sh_{El}, POCC, p_{H2O}, p_{POD}	-	-	-
$\overrightarrow{MARKET}_D$	Hydrogen price: p_{hy}	7.8	€ kg^{-1}	Based on mean price of (EEX, 2026)
	Electricity reference value: RV	73.5	€ MWh^{-1}	Federal Office of Justice (2026)
$\overrightarrow{OP}$	ObservPeriod	25	years	-

The energy system for the operation optimization modeled in oemof, is schematically shown in Figure 6.

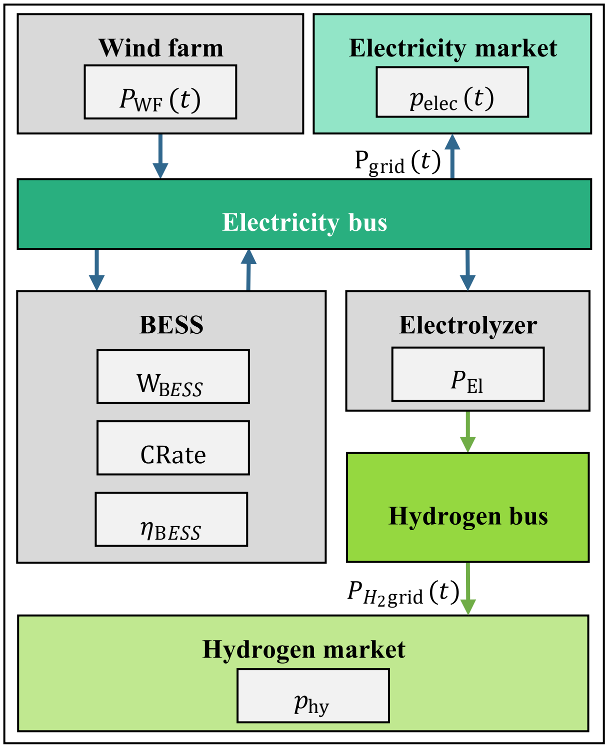

Figure 6: Schematic overview of the modeled energy system for the operation optimization in oemof.

The power generated by the WF at a timestep $P_{\mathrm{WF}}(t)$ is fed into an electricity bus. At the electricity bus the sum of all in- and outgoing flows must be zero for all t. The electricity bus is connected to a battery with a fixed capacity C_{BESS}, a C-rate CRate, and an overall storage efficiency η_{BESS}. Electricity can be sold at the electricity market or fed into the electrolyzer with a fixed rated power P_{El}. The time varying electricity price $p_{\mathrm{elec}}(t)$ consist of hourly day-ahead market data from Germany in 2024 (Energy-Charts, 2026). The produced hydrogen can be sold to the hydrogen market for a fixed hydrogen price p_{hy} of 7.8 € kg^{-1} equals , which was the average price for hydrogen in 2024 of the HYDRIX (EEX, 2026).

3.2 Design optimization

This section presents the results of the design optimization method introduced in Sect. 2.2, applied to the case study described in the previous Sect. 3.1, noting that the operational optimization of Sect. 2.3 has not been performed at this stage. Due to the described model of the electrolyzer efficiency, degradation, stack replacement, and degradation evaluation, the design optimization problem is nonlinear. In the context of nonlinear and non-convex optimization, it is generally only possible to identify local optima. Demonstrating that the global optimum has been found is considerably more challenging (Kallrath, 2013). However, to identify a near-optimal solution the design space is explored by varying the design variables P_{El} and W_{BESS} within the DE optimization algorithm. The panels of Figure 7 depict the variable space, ranging from 0 to 30 % of the WF's rated power on each axis. The central panel shows the AP with the hydrogen price assumed in the use case described in Sect. 3.1. The left and right heat maps are also showing the AP for deviating hydrogen prices.

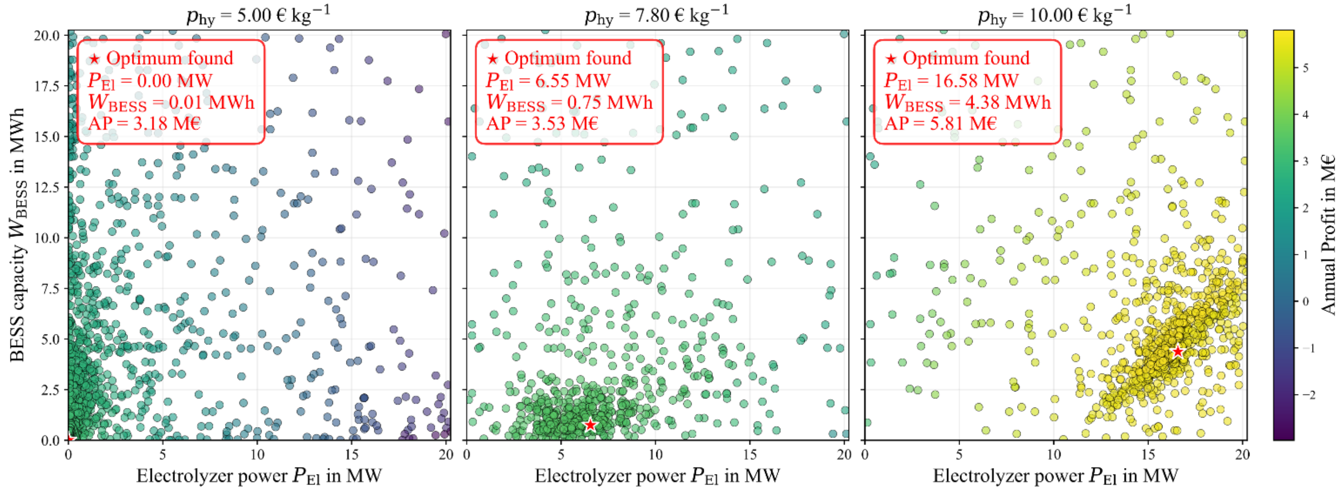

Figure 7: Design space exploration of annual profit via differential evolution for three different hydrogen prices.

Figure 7 illustrates the strong dependence of the optimal HPP design on the assumed hydrogen price. The results indicate that the optimum found shifts toward larger electrolyzer and BESS capacities as the hydrogen price increases. With a constant hydrogen price of 5.0 € kg^{-1}, the maximum AP occurs at neglectable electrolyzer and BESS sizes, because the stand-alone WF remains the more profitable option. This AP without electrolyzer and BESS is calculated as the product of AEP and the difference between the RV and the LCOE amounting to 3.21 M€ a^{-1}. As seen in the middle and right panels of Figure 7 the hydrogen price of 7.8 € kg^{-1}, results in an optimal configuration shift to 6.55 MW and 0.75 MWh, while at 10 € kg^{-1} it further increases to 16.58 MW and 4.38 MWh. The optimum identified in the central panel of Figure 7 with p_{hy} equals 7.8 € kg^{-1} serves as configuration for the following observations. Additional results as the mean AP, mean annual revenues, mean AHP, and TOTEX determined over the observation period, are detailed in Table 2.

Table 2: Design optimization results of the described use case over the entire observation period.

Output	Value	Unit
Mean AP	3.53	M€ a^{-1}
Mean annual hydrogen profit	1.09	M€ a^{-1}
Mean annual electricity profit	2.44	M€ a^{-1}
Mean AHP	642	t a^{-1}
Mean annual hydrogen revenue	5.01	M€ a^{-1}
Mean annual electricity revenue	9.81	M€ a^{-1}
LCOH	6.11	€ $\mathrm{kg_{H_2}}^{-1}$
TOTEX without WF	45.84	M€

TOTEX electrolyzer	42.10	M€
TOTEX pipeline system incl. water supply	1.59	M€
TOTEX electricity supply	1.39	M€
TOTEX BESS	0.76	M€

The AP of 3.53 M€ a^{-1} of the HPP is composed of the annual electricity profit by a share of approximately two-third and the annual hydrogen profit by one-third. For the given hydrogen price, the AP of the HPP is about 10 % above the AP of the stand-alone WF, demonstrating that the HPP can have a significant impact on the economics of the system installed at the given WF site. The annual electricity revenue accounts for 9.81 M€ a^{-1}, representing approximately two thirds of the total revenues, while hydrogen sales contribute the remaining one third with 5.01 M€ a^{-1}, which is consistent with the relative contributions to the AP. The TOTEX without the existing WF respectively of the added hydrogen system amount to 45.84 M€ over the entire observation period. The largest share of TOTEX is associated with the electrolyzer, driven primarily by variable electrolyzer OPEX in the form of electricity procurement costs, which account for about 69 % of the electrolyzer TOTEX. The remaining costs are significantly lower. This cost distribution emphasizes that the profit optimization of the HPP depends primarily on the electricity procurement and secondary on the electrolyzer investment and replacement costs, rather than on the cost reduction of peripheral components.

To assess the impact of the modified electrolyzer modeling and the inclusion of a BESS by avoiding the strong price sensitivity the LCOH of the method of Reichartz et al. (2024a) is compared with the LCOH obtained in this study, accounting for the part-load efficiency and degradation of the electrolyzer and different BESS sizes. Figure 8 presents the calculated minimum LCOH plotted against the ratio of P_{El} to P_{WF}.

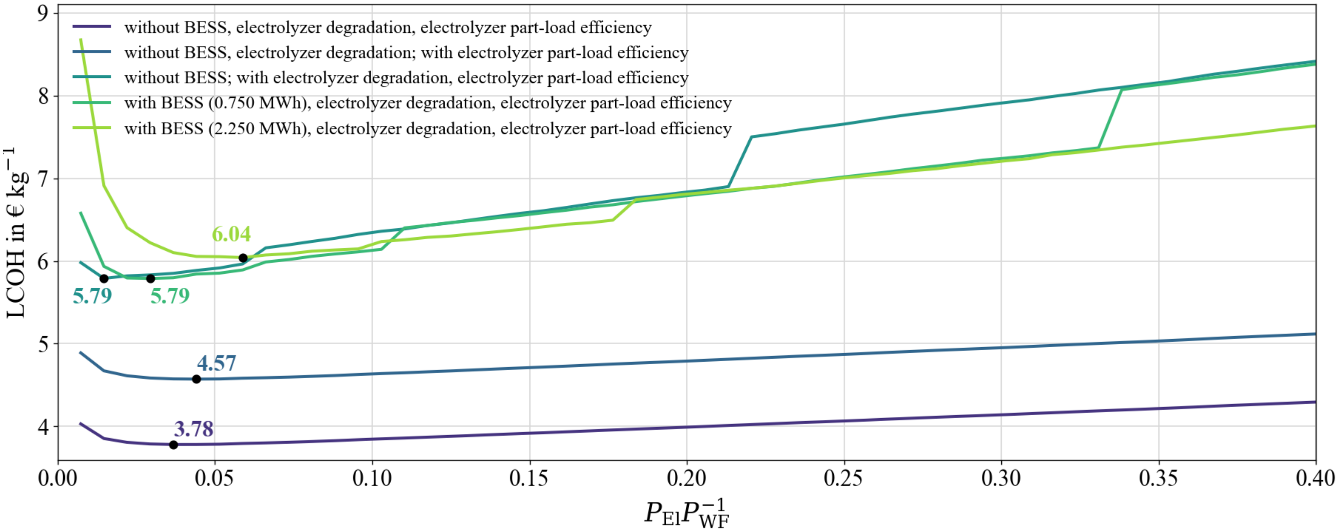

Figure 8: LCOH over the ratio of electrolyzer rated power to wind farm rated power for four different modeling approaches and two different BESS sizes.

A comparison of the minimum LCOH values of the model variants without BESS shows that neglecting electrolyzer degradation leads to an underestimation of the LCOH by approximately 21 %, while neglecting both degradation and partial-load efficiency results in an underestimation of about 35 %. These results highlight the critical importance of accurately representing both degradation effects and part-load efficiency in electrolyzer modeling. By adding a BESS capacity of 0.75 MWh, that was previously identified as optimum for the AP maximization for the given use case, the LCOH remain at a constant level while the AP increases by 7 % in this scenario. While the incremental hydrogen yield is sufficient to offset the additional BESS-related TOTEX, resulting in constant LCOH, the system benefits from enhanced operational flexibility. Consequently, the BESS effectively increases the AP by capturing higher market revenues. An increased BESS capacity shifts the LCOH minimum to higher electrolyzer capacities while increasing LCOH. Ultimately, these findings underscore that the choice of the objective function is pivotal for the optimal sizing of both the electrolyzer and the BESS, as it fundamentally dictates whether the integration of a BESS is perceived as a profit benefit or a cost driver.

A technical driver behind this economic trade-off is the BESS ability to mitigate electrolyzer degradation. Specifically, the operation strategy assumed in Sect. 2.2.1 results in an annual electrolyzer degradation, calculated according to Sect. 2.2.2, for the in Sect. 3.1 presented HPP system of $0.1294\ \mathrm{V\ a^{-1}}$. This TAD corresponds to degradation costs of $0.590\ \mathrm{M€\ a^{-1}}$, when converted according to Eq. (24). If the BESS is removed, the TAD increases to $0.1577\ \mathrm{V\ a^{-1}}$, increasing the degradation cost by $0.129\ \mathrm{M€\ a^{-1}}$. The electrolyzer degradation with and without BESS divides into the different operation modes according to Table 3.

Table 3: Share of the total annual electrolyzer degradation depending on the electrolyzer operation modes with and without BESS.

Operation mode	With BESS (0.75 MWh): $\mathrm{TAD} = 0.1294\ \mathrm{V\ a^{-1}}$		Without BESS: $\mathrm{TAD} = 0.1577\ \mathrm{V\ a^{-1}}$	
	AD in $\mathrm{V\ a^{-1}}$	AD share of TAD in %	AD in $\mathrm{V\ a^{-1}}$	AD share of TAD in %
rated	0.0145	11.18	0.0145	9.17
partl	0.0012	0.96	0.0009	0.56
off	0.0021	1.61	0.0026	1.63
fluct	0.0675	52.19	0.0666	42.21
stop	0.0441	34.06	0.0732	46.43

The fluctuating operation mode is the dominant driver of electrolyzer degradation in the system with BESS. However, removing the BESS leads to a significant increase in the TAD by more than a fifth. This is primarily driven by the degradation from start-stop cycles, which increases by about 60 %. Furthermore, the AP of the System without BESS decreases to 3.4 M€, representing a 3.7 % reduction compared to the configuration featuring a 0.75 MWh BESS. These findings underline the effectiveness of the BESS within the implemented operation strategy by buffering volatile WF power. The battery prevents frequent shutdowns and ensures a more continuous hydrogen production, thereby substantially mitigating cycle-induced degradation of the electrolyzer. While the BESS integration entails additional CAPEX, these costs are offset over the system's operational period by reduced electrolyzer degradation costs and increased hydrogen revenues, even when limited to a buffering operation strategy.

3.3 MIL operation optimization

As described in Section 1, the design and operation of electrolyzers are inherently interdependent. In the design optimization method presented in this study, an operational strategy for the electrolyzer and the BESS is assumed following Section 2.2.2. This assumption is evaluated in this Section by comparing the electrolyzer and BESS operation obtained from the design optimization with the results of the MIL operation optimization introduced in Sect. 2.3 and a subsequent degradation evaluation of Sect. 2.2.2. Figure 9 presents the OAP and its decomposition into annual electricity and hydrogen revenues as well as water supply and degradation costs for both optimization approaches of the first year for operation under constant and variable electricity prices.

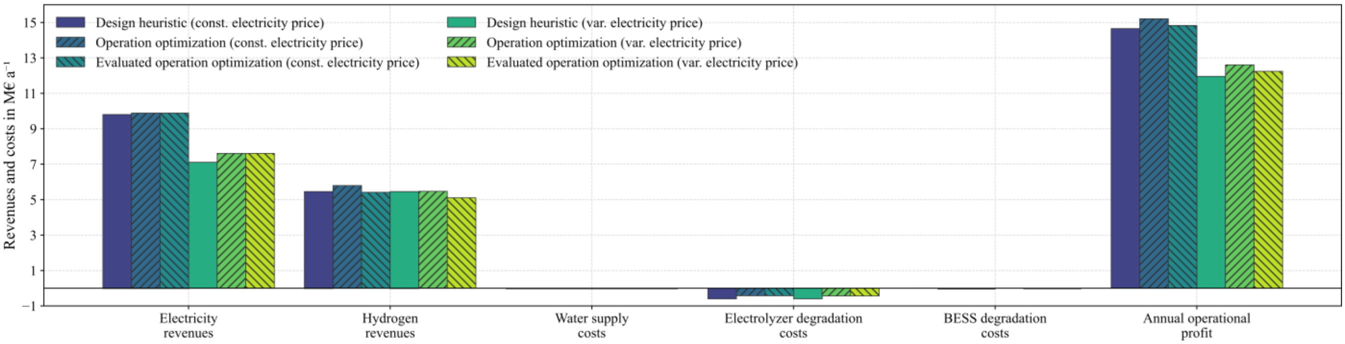

Figure 9: Comparison of the annual operational profit and its shares of the design optimization, the MIL operation optimization, and its degradation evaluation for constant and variable electricity prices.

Figure 9 shows that the assumed constant electricity price in the design optimization leads to a systematic overestimation of electricity revenues and, consequently, of the OAP by 23 % when compared to variable electricity price conditions of 2024. This highlights the limitations of design-stage economic assumptions when applied to real-world market environments with pronounced price volatility. In addition, the electrolyzer degradation costs associated with the operating strategy assumed during the design optimization amount to 0.59 M€ $a^{-1}$and can be reduced by about 38 % through the proposed operational optimization under variable price conditions. This reduction underlines the strong influence of operational control on component ageing and long-term economic performance. In contrast, the BESS undergoes approximately one cycle per day under the variable price operation optimization. Given a nominal cycle life of 8,000 cycles, this operational frequency corresponds to an expected service life of around 22 years. Consequently, the resulting BESS degradation costs are minor compared to both the OAP and the electrolyzer degradation costs, as seen in Fig. 9. Furthermore, this evaluation indicates that the baseline assumption of a 10-year lifetime utilized during the design optimization is highly conservative.

Neglecting degradation-induced efficiency losses and using a piecewise linearized efficiency of the electrolyzer within the operation optimization leads to an overestimation of hydrogen revenues by 7 % under variable electricity price conditions, relative to the revenues obtained from the subsequent degradation evaluation. Initially, the MIL operation optimization suggests a significant economic potential, with a projected OAP approximately 5 % higher than that of the design heuristic. Despite the subsequent revenue correction due to degradation effects and efficiency linearization, the evaluated OAP remains above the value calculated in the design phase, reaching 102 % under variable electricity prices and 101 % under constant electricity prices. This demonstrates that MIL operational optimization, even when neglecting degradation-related efficiency losses, can slightly enhance economic performance relative to the simplified operation assumptions in the design optimization. However, the gap between the initial 5 % projection and the evaluated 1 % to 2 % gain highlights the potential for further improvements through a more comprehensive representation of degradation effects within the economically optimum operation of the HPP.

To analyse the impact of the assumed hydrogen price on the optimal HPP operation and to evaluate the discrepancies between the system components operation of the design optimization and the MIL operation optimization, Figure 10 presents different annual load duration curves. The figure illustrates the electrolyzer power input for varying hydrogen price scenarios alongside the WF power output. Additionally, the day-ahead electricity market price of 2024 is included and plotted in descending order.

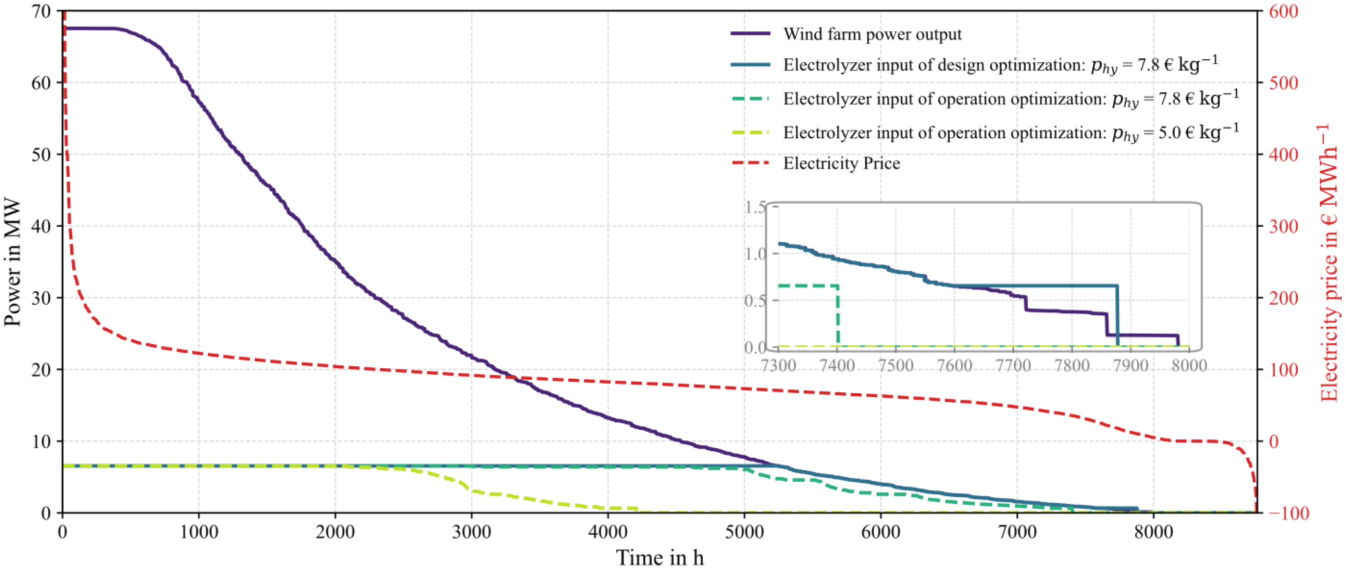

Figure 10: Sorted load duration curves of the WF power output, the electrolyzer power input of the design optimization, and for the MIL operation optimization for two different hydrogen price scenarios, and the sorted electricity price over one year.

The comparative analysis of the sorted load duration curves, as illustrated in Figure 10, reveals that the operational characteristics of the design heuristic and the operational optimization differ marginally at a hydrogen price of 7.8 € kg^{-1}. Specifically, the design heuristic (solid blue line) accounts for 6,375 full load hours (FLH) per year, while the operational optimization (dashed teal line) reaches 5,892 FLH. This high degree of similarity is primarily attributed to the fact that the assumed hydrogen price is significantly higher than the average electricity day-ahead market price of 79.6 € MWh^{-1}. Under these conditions, the marginal revenue from hydrogen production mostly exceeds the opportunity costs of direct electricity sales, incentivizing the system to maximize hydrogen output regardless of the specific operation approach. However, when reducing the hydrogen price to 5.0 € kg^{-1} (dashed light green line), the optimized electrolyzer operation shifts to 3,157 FLH. Despite the design operation strategy's price-independent nature and the resulting inability to account for fluctuating market signals, the evaluated OAP achieved through MIL optimization exceeds that of the static design operation under variable price conditions by more than 9 % at the lower hydrogen price scenario. This suggests that the heuristic remains active during periods where market electricity prices exceed the marginal revenue of hydrogen production, resulting in associated economic losses compared to the price-dependent MIL operation optimization. It must be noted, however, that the results of the operation heuristic compared to the design optimization observed here are specific to the investigated use case.

4 Discussion and future work

4.1 Design optimization methodology advancements

This study extends the optimization framework for co-located wind-hydrogen systems developed by Reichartz et al. (2024b). A significant advancement is the integration of an empirical electrolyzer model from Han et al. (2015) and Abdin et al. (2015) that calculates electrolyzer efficiency as a function of cell voltage and Faraday efficiency. Degradation of the electrolyzer depending on five different operating modes was added as by increasing the electrolyzer cell voltage and therefore decreasing efficiency. To reduce the electrolyzer degradation a BESS operating as an electricity buffer is added into the HPP. The objective function was shifted from LCOH to AP allowing a more comprehensive economic assessment. By integrating revenue structures for both hydrogen and electricity sales, it was demonstrated that approximately two-thirds of the total AP is generated through electricity revenues, while one-third stems from hydrogen sales. Electricity procurement costs were identified as the primary driver of the hydrogen system's TOTEX, aligning with results reported by Nachit et al. (2026). Despite these operational costs, the HPP configuration demonstrates economic advantages under the assumed energy price scenario. Specifically, the AP of a stand-alone WF is approximately 9 % lower than that of the optimal HPP investigated in this use case. This margin underscores the potential of hybridization to enhance the economic efficiency of a given WF site. Consequently, these findings are of particular relevance for WF operators and project planners aiming to evaluate the viability of extending existing or planned WFs with decentralized PEM electrolysis and BESS. By providing a methodology that balances capital investment against operational flexibility and component degradation, the method enables a risk-adjusted assessment of integrated energy systems by keeping site specific costs into account. In this context, the design optimization identified a near-optimal solution for the electrolyzer rated power and BESS capacity of the investigated use case. This optimum electrolyzer rated power was found to be close to 10 % power relative to the installed WF power, that is also within the optimum range of electrolyzer power found by Chatzistlyianos et al. (2025).

To evaluate the operation and the resulting revenues within the design methodology, a fixed operation strategy for the electrolyzer and the BESS was developed. This strategy prioritizes maximizing the AHP to effectively reduce the LCOH using WF power exclusively, while minimizing degradation intense start-stop cycles by the BESS. By mapping electrolyzer degradation across five distinct operational modes, this study introduces a method to evaluate cumulative annual degradation. The results underscore that degradation leads to a 21 % underestimation of the LCOH, which increases to 35 % when part-load efficiency is also ignored. For project planners, these findings are crucial to avoid overly optimistic economic forecasts. Furthermore, the results show that while a BESS can reduce the annual degradation by a fifth the LCOH remain constant, highlighting that the choice of the objective function exerts a profound influence on the optimal HPP design and underscores the necessity of precise BESS dimensioning. While the BESS effectively protects the electrolyzer stack from premature aging, the BESS itself is subject to wear-and-tear through cycling (Xu et al., 2018). BESS degradation, however, was only implicitly accounted for in the design method through a conservative assumption of a calendar life of 10 years. Cycle-induced BESS degradation was not explicitly modelled but could lead to an increase in LCOH. This may obscure a trend observed by Chatzistlyianos et al. (2025), where BESS integration consistently increases the LCOH. Furthermore, this study assumes a pure buffering strategy for the BESS. In reality, multi-market BESS can generate significant additional value through revenue stacking, such as participating in frequency regulation or energy arbitrage (Mohamed et al., 2023). While such strategies could enhance the overall economic performance of the HPP, they would also increase battery cycling and further complicate the operational dispatch. Including these multi-market opportunities alongside BESS degradation costs would likely shift the optimum economical BESS capacity and require further operation strategies to balance the trade-off between electrolyzer protection and battery health.

4.2 Operation strategy comparison

To demonstrate the profit potential of the assumed operation strategy in the design optimization method, a MIL operation optimization was performed for the designed system. This comparative approach is particularly valuable for system analysts and project developers, as it quantifies the performance gap between simplified heuristic dispatch and mathematically optimal operation. By maximizing the operation-dependent profit under variable market prices conditions over one year, a profit increase to 107 % was identified. However, the MIL operation optimization uses a piecewise linearization of the part-load efficiency and neglects the direct impact of degradation on the electrolyzers efficiency during the decision-making process. A subsequent evaluation of the operation optimization results, which factored these effects back in, showed that the actual profit gain was reduced to 102 % relative to the design optimization OAP. This profit discrepancy highlights that idealized optimization results must be critically verified against physical degradation models to establish realistic business cases and avoid overestimating long-term revenues. To refine these results, a MIL rolling-horizon optimization approach like the one from Chen et al. (2024) could present a viable solution to incorporate these degradation-related efficiency losses in shorter intervals. This would allow the operational strategy to adapt to the aging of the electrolyzer stacks more realistic. Alternatively, nonlinear optimization could directly integrate degradation effects into the decision-making process, although this significantly increases computational effort. Implementing more sophisticated allocation approaches, such as rotating or daisy-chain stack usage, could further mitigate degradation and enhance revenues (Zhou et al., 2025; Cheng et al., 2025). However, such refinements would simultaneously increase the model complexity and the associated computational burden. Additionally, this work did not explore variations in electricity price profiles or wind generation time series. These external drivers can exert a substantial influence not only on the optimal operating behaviour, but also on the resulting component sizing configurations and the performance gap between the rule-based heuristic and the MILP dispatch optimization. In markets with high price volatility or different meteorological characteristics, the divergence between static rules and adaptive optimization might increase significantly, potentially limiting the transferability of these findings. To derive reliable investment decisions, a hybrid wind farm design must demonstrate robustness against external factors. Therefore, the integration of adaptive operational optimization directly into the sizing process can ensure that the system responds to market volatility or volatile wind power generation, providing a basis for identifying the optimal HPP design even under uncertain external conditions.

Code and data availability

No data other than that given in the paper are required to produce the presented results. The source code is not published.

Author contributions

The concept and method of the present study were developed by DF, TR, and LB. DF and TR performed the initial implementation of the software, which was extended and improved by TP. DF and TP performed the initial text creation. TR, MK, and GJ were responsible for supervision, revision, and final approval. All authors have read and agreed to the published version of the paper.

Competing interests

The contact author has declared that none of the authors has any competing interests.

Disclaimer

Copernicus Publications remains neutral with regard to jurisdictional claims made in the text, published maps, institutional affiliations, or any other geographical representation in this paper. While Copernicus Publications makes every effort to include appropriate place names, the final responsibility lies with the authors. Views expressed in the text are those of the authors and do not necessarily reflect the views of the publisher.

Acknowledgements

AI was used to assist with language and phrasing for some text parts of the manuscript.

Financial support

This research has been supported by the German Federal Ministry for Economic Affairs and Energy (grant no. 03EN3103A). The open-access publication was funded by the Open Access Publication Fund of RWTH Aachen University.

Review statement

5 References

Abdin, Z., Webb, C. J., and Gray, E.: Modelling and simulation of a proton exchange membrane (PEM) electrolyser cell, Int. J. Hydrogen Energy, 40, 13243–13257, https://doi.org/10.1016/j.ijhydene.2015.07.129, 2015.

anemos: Wind and Yield Index Report, https://www.windindustrie-in-deutschland.de/publikationen/fachartikel/anemos-wind-und-ertragsindex-report-2024, last access: 2 June 2026, 2024.

Balderrama, S., Lombardi, F., Riva, F., Canedo, W., Colombo, E., and Quoilin, S.: A two-stage linear programming optimization framework for isolated hybrid microgrids in a rural context: The case study of the "El Espino" community, Energy, 188, 116073, https://doi.org/10.1016/j.energy.2019.116073, 2019.

Bechmann, A. and Quick, J.: Market-Driven Wind Resource Assessment, J. Phys.: Conf. Ser., 3025, 12001, https://doi.org/10.1088/1742-6596/3025/1/012001, 2025.

Bockelmann, M., Becker, M., Stypka, S., Bauer, S., Minke, C., and Turek, T.: Erzeugung von Wasserstoff durch Elektrolyse, Chem. Unserer Zeit, 58, 29–45, https://doi.org/10.1002/ciuz.202300024, 2024.

Bosch: Hybrion PEM-Elektrolysis Stack, https://www.bosch-hydrogen-energy.com/media/pem_electrolysis/hybrion_pem_electrolysis_stacks/bosch-hybrion-pem-electrolysis-stacks-specification-sheet.pdf, last access: 2 June 2026, 2025.

Bošnjaković, M., Katinić, M., Santa, R., and Marić, D.: Wind Turbine Technology Trends, Appl. Sci., 12, 8653, https://doi.org/10.3390/app12178653, 2022.

Buttler, A. and Spliethoff, H.: Current status of water electrolysis for energy storage, grid balancing and sector coupling via power-to-gas and power-to-liquids: A review, Renew. Sust. Energ. Rev., 82, 2440–2454, https://doi.org/10.1016/j.rser.2017.09.003, 2018.

Canbulat, S., Balci, K., Canbulat, O., and Bayram, I. S.: Techno-Economic Analysis of On-Site Energy Storage Units to Mitigate Wind Energy Curtailment: A Case Study in Scotland, Energies, 14, 1691, https://doi.org/10.3390/en14061691, 2021.

Carmo, M., Fritz, D. L., Mergel, J., and Stolten, D.: A comprehensive review on PEM water electrolysis, Int. J. Hydrogen Energy, 38, 4901–4934, https://doi.org/10.1016/j.ijhydene.2013.01.151, 2013.

Chatzistlyianos, E., Psarros, G., Chinaris, P., and Papathanassiou, S.: Cost Estimation for Green Hydrogen Production and Distribution, in: 2025 21st International Conference on the European Energy Market (EEM), Lisbon, Portugal, 27-29 May 2025, 1–6, 2025.

Chen, R., Gao, C., and Ming, H.: Rolling-horizon optimization strategy for wind-storage system in electricity market, IET Renew. Power Gener., 18, 825–836, https://doi.org/10.1049/rpg2.12954, 2024.

Cheng, K., He, S., and Hu, B.: Power adaptive control strategy for multi-stack PEM photovoltaic hydrogen systems considering electrolysis unit efficiency and hydrogen production rate, Sust. Energy Technol. Assess., 75, 104200, https://doi.org/10.1016/j.seta.2025.104200, 2025.

Cole, W., Ramasamy, V., and Turan, M.: Cost Projections for Utility-Scale Battery Storage: 2025 Update, Golden, CO 80401, NREL/TP-6A40-93281, 2025.

Cozzolino, R. and Bella, G.: A review of electrolyzer-based systems providing grid ancillary services: current status, market, challenges and future directions, Front. Energy Res., 12, 1358333, https://doi.org/10.3389/fenrg.2024.1358333, 2024.

Dolatabadi, A., Ebadi, R., and Mohammadi-Ivatloo, B.: A Two-Stage Stochastic Programming Model for the Optimal Sizing of Hybrid PV/diesel/battery in Hybrid Electric Ship System, Journal of Operation and Automation in Power Engineering, 7, 16–26, https://doi.org/10.22098/joape.2019.4395.1349, 2019.

EEX: Hydrogen, https://www.eex.com/en/markets/hydrogen, last access: 16 January 2026, 2026.

Eltamaly, A. M. and Almutairi, Z. A.: Nested Optimization Algorithms for Accurately Sizing a Clean Energy Smart Grid System, Considering Uncertainties and Demand Response, Sustainability, 17, 2744, https://doi.org/10.3390/su17062744, 2025.

Energy-Charts: Spot Market Prices, Fraunhofer ISE, https://www.energy-charts.info/charts/price_spot_market/chart.htm?l=en&c=DE&interval=year&year=2024&minuteInterval=60min&legendItems=ey5, last access: 16 January 2026, 2026.

European Parliament and Council: REGULATION (EU) 2021/1119 OF THE EUROPEAN PARLIAMENT AND OF THE COUNCIL of 30 June 2021 establishing the framework for achieving climate neutrality and amending Regulations (EC) No 401/2009 and (EU) 2018/1999 ('European Climate Law'): European Climate Law (Reg. (EU) 2021/1119), 2021.

Fabianek, P. and Madlener, R.: Techno-economic analysis and optimal sizing of hybrid PV-wind systems for hydrogen production by PEM electrolysis in California and Northern Germany, Int. J. Hydrogen Energy, 67, 1157–1172, https://doi.org/10.1016/j.ijhydene.2023.11.196, 2024.

Federal Network Agency: Hydrogen core network, https://www.bundesnetzagentur.de/EN/Areas/Energy/HydrogenCoreNetwork/start.html, last access: 15 January 2026, 2026.

Federal Office of Justice: § 85a EEG 2023, https://www.gesetze-im-internet.de/eeg_2014/__85a.html, last access: 16 January 2026, 2026.

Frensch, S. H., Fouda-Onana, F., Serre, G., Thoby, D., Araya, S. S., and Kær, S. K.: Influence of the operation mode on PEM water electrolysis degradation, Int. J. Hydrogen Energy, 44, 29889–29898, https://doi.org/10.1016/j.ijhydene.2019.09.169, 2019.

García-Valverde, R., Espinosa, N., and Urbina, A.: Simple PEM water electrolyser model and experimental validation, Int. J. Hydrogen Energy, 37, 1927–1938, https://doi.org/10.1016/j.ijhydene.2011.09.027, 2012.

Görgün, H.: Dynamic modelling of a proton exchange membrane (PEM) electrolyzer, Int. J. Hydrogen Energy, 31, 29–38, https://doi.org/10.1016/j.ijhydene.2005.04.001, 2006.

Grant, E., Brunik, K., King, J., and Clark, C. E.: Hybrid power plant design for low-carbon hydrogen in the United States, J. Phys.: Conf. Ser., 2767, 82019, https://doi.org/10.1088/1742-6596/2767/8/082019, 2024.

Gurobi Optimization: Nonlinear Constraints - Gurobi Optimizer Reference Manual, https://docs.gurobi.com/projects/optimizer/en/current/features/nonlinear.html#subsubsectiongenconstrfunctionpwl, last access: 2 February 2026, 2026.

Han, B., Steen, S. M., Mo, J., and Zhang, F.-Y.: Electrochemical performance modeling of a proton exchange membrane electrolyzer cell for hydrogen energy, Int. J. Hydrogen Energy, 40, 7006–7016, https://doi.org/10.1016/j.ijhydene.2015.03.164, 2015.

Hernández-Gómez, Á., Ramirez, V., and Guilbert, D.: Investigation of PEM electrolyzer modeling: Electrical domain, efficiency, and specific energy consumption, Int. J. Hydrogen Energy, 45, 14625–14639, https://doi.org/10.1016/j.ijhydene.2020.03.195, 2020.

Hilpert, S., Kaldemeyer, C., Krien, U., Günther, S., Wingenbach, C., and Plessmann, G.: The Open Energy Modelling Framework (oemof) - A new approach to facilitate open science in energy system modelling, Energy Strategy Rev., 22, 16–25, https://doi.org/10.1016/j.esr.2018.07.001, 2018.

Hofrichter, A., Rank, D., Heberl, M., and Sterner, M.: Determination of the optimal power ratio between electrolysis and renewable energy to investigate the effects on the hydrogen production costs, Int. J. Hydrogen Energy, 48, 1651–1663, https://doi.org/10.1016/j.ijhydene.2022.09.263, 2023.

Ibáñez-Rioja, A., Puranen, P., Järvinen, L., Kosonen, A., Ruuskanen, V., Hynynen, K., Ahola, J., and Kauranen, P.: Baseload hydrogen supply from an off-grid solar PV–wind power–battery–water electrolyzer plant, Energy, 322, 135304, https://doi.org/10.1016/j.energy.2025.135304, 2025.

IRENA: Renewable power generation costs in 2023, https://www.irena.org/Publications/2024/Sep/Renewable-Power-Generation-Costs-in-2023, last access: 6 March 2026, 2024.

IRENA: Green hydrogen cost reduction, https://h2.pe/uploads/IRENA_Green_hydrogen_cost_2020.pdf, last access: 2 June 2026, 2020.

Kallrath, J.: Gemischt-ganzzahlige Optimierung: Modellierung in der Praxis, Springer Fachmedien Wiesbaden, Wiesbaden, 2013.

Kansara, R. and Roldán Serrano, M. I.: Coupled Design and Operation Optimization for Decarbonization of Industrial Energy Systems Using an Open-Source In-House Tool, Eng, 5, 3033–3048, https://doi.org/10.3390/eng5040158, 2024.

Krien, U., Schönfeldt, P., Launer, J., Hilpert, S., Kaldemeyer, C., and Pleßmann, G.: oemof.solph—A model generator for linear and mixed-integer linear optimisation of energy systems, Software Impacts, 6, 100028, https://doi.org/10.1016/j.simpa.2020.100028, 2020.

Kurzweil, P. and Dietlmeier, O. K.: Elektrochemische Speicher, Springer Fachmedien Wiesbaden, Wiesbaden, 2018.

Lim, D., Lee, B., Lee, H., Byun, M., Cho, H.-S., Cho, W., Kim, C.-H., Brigljević, B., and Lim, H.: Impact of voltage degradation in water electrolyzers on sustainability of synthetic natural gas production: Energy, economic, and environmental analysis, Energy Convers. Manage., 245, 114516, https://doi.org/10.1016/j.enconman.2021.114516, 2021.

Lu, X., Du, B., Zhou, S., Zhu, W., Li, Y., Yang, Y., Xie, C., Zhao, B., Zhang, L., Song, J., and Deng, Z.: Optimization of power allocation for wind-hydrogen system multi-stack PEM water electrolyzer considering degradation conditions, Int. J. Hydrogen Energy, 48, 5850–5872, https://doi.org/10.1016/j.ijhydene.2022.11.092, 2023.

Lynus: Lynus Batteriespeichersystem, https://shop-eu.lynus.io/WebRoot/epagesDE/Shops/lynus/679B/9A1C/E513/585D/F8BA/0A0C/05B7/B53A/Lynus_Batteriespeicher_Containerlosung_500kW___1MWh.pdf, last access: 12 May 2026, 2026.

Makhsoos, A., Kandidayeni, M., Pollet, B. G., and Boulon, L.: Proton exchange membrane water electrolyzers degradation models review: implications for power allocation and energy management, J. Power Soruces, 655, 238003, https://doi.org/10.1016/j.jpowsour.2025.238003, 2025.

Mohamed, A., Rigo-Mariani, R., Debusschere, V., and Pin, L.: Stacked revenues for energy storage participating in energy and reserve markets with an optimal frequency regulation modeling, Applied Energy, 350, 121721, https://doi.org/10.1016/j.apenergy.2023.121721, 2023.

Nachit, I., Naanani, H., and Ikharrazne, L.: Dynamic and techno-economic assessment of electrolyser technologies under intermittent renewable energy: Performance and cost competitiveness across six countries, Int. J. Hydrogen Energy, 201, 152841, https://doi.org/10.1016/j.ijhydene.2025.152841, 2026.

Nel: PEM Electrolyser - PEM Series, https://nelhydrogen.com/product/psm-series-electrolyser/, last access: 1 June 2026, 2025.

New European Wind Atlas: Welcome to the New European Wind Atlas, https://map.neweuropeanwindatlas.eu/, last access: 15 January 2026, 2026.

OECD Economic Surveys: European Union and Euro Area 2025, 2025, OECD Publishing, 2025.

Papakonstantinou, G., Algara-Siller, G., Teschner, D., Vidaković-Koch, T., Schlögl, R., and Sundmacher, K.: Degradation study of a proton exchange membrane water electrolyzer under dynamic operation conditions, Applied Energy, 280, 115911, https://doi.org/10.1016/j.apenergy.2020.115911, 2020.

Peng, J., Vijayshankar, S., King, J., and Mathieu, J.: Trade-offs between Battery Energy Storage and Hydrogen Storage in Off-Grid Green Hydrogen Systems, in: Proceedings of the 57th Hawaii International Conference on System Sciences, 3097, 2025.

Reichartz, T., Jacobs, G., Rathmes, T., Blickwedel, L., and Schelenz, R.: Optimal position and distribution mode for on-site hydrogen electrolyzers in onshore wind farms for a minimal levelized cost of hydrogen (LCoH), Wind Energ. Sci., 9, 281–295, https://doi.org/10.5194/wes-9-281-2024, 2024a.

Reichartz, T., Jacobs, G., Blickwedel, L., Frings, D., and Schelenz, R.: Co-Design of a Wind–Hydrogen System: The Effect of Varying Wind Turbine Types on Techno-Economic Parameters, Energies, 17, 4710, https://doi.org/10.3390/en17184710, 2024b.

Reuß, M. E.: Techno-ökonomische Analyse alternativer Wasserstoffinfrastruktur, Ph.D. thesis, RWTH Aachen University, 2019.

Robinius, M., Otto, A., Heuser, P., Welder, L., Syranidis, K., Ryberg, D., Grube, T., Markewitz, P., Peters, R., and Stolten, D.: Linking the Power and Transport Sectors—Part 1: The Principle of Sector Coupling, Energies, 10, 956, https://doi.org/10.3390/en10070956, 2017.

Roscher, B.: Multi-dimensional wind farm optimization in the concept phase, Ph.D. thesis, RWTH Aachen University, 2020.

Rozzi, E., Grimaldi, A., Minuto, F. D., and Lanzini, A.: Model complexity and optimization trade-offs in the design and scheduling of hybrid hydrogen-battery systems, Energy Convers. Manage., 344, 120306, https://doi.org/10.1016/j.enconman.2025.120306, 2025.

Sayed-Ahmed, H., Toldy, Á., and Santasalo-Aarnio, A.: Dynamic operation of proton exchange membrane electrolyzers—Critical review, Renew. Sust. Energ. Rev., 189, 113883, https://doi.org/10.1016/j.rser.2023.113883, 2024.

Schnuelle, C., Wassermann, T., Fuhrlaender, D., and Zondervan, E.: Dynamic hydrogen production from PV & wind direct electricity supply – Modeling and techno-economic assessment, Int. J. Hydrogen Energy, 45, 29938–29952, https://doi.org/10.1016/j.ijhydene.2020.08.044, 2020.

Shams, M. H., Niaz, H., Na, J., Anvari-Moghaddam, A., and Liu, J. J.: Machine learning-based utilization of renewable power curtailments under uncertainty by planning of hydrogen systems and battery storages, J. Energy Storage, 41, 103010, https://doi.org/10.1016/j.est.2021.103010, 2021.

Shiva Kumar, S. and Himabindu, V.: Hydrogen production by PEM water electrolysis – A review, Mater. Sci. Energy Technol., 2, 442–454, https://doi.org/10.1016/j.mset.2019.03.002, 2019.

Smolinka, T., Wiebe, N., Sterchele, P., Palzer, A., Lehner, F., Jansen, M., Kiemel, S., Miehe, R., Wahren, S., and Zimmermann, F.: Industrialisierung der Wasserelektrolyse in Deutschland: Chancen und Herausforderungen für nachhaltigen Wasserstoff für Verkehr, Strom und Wärme, https://www.ipa.fraunhofer.de/de/Publikationen/studien/studie-industrialisierung-wasserelektrolyse.html, last access: 2 June 2026, 2018.

Storn, R. and Price, K.: Differential Evolution – A Simple and Efficient Heuristic for global Optimization over Continuous Spaces, J. Glob. Optim., 11, 341–359, https://doi.org/10.1023/A:1008202821328, 1997.

Tezer, T.: Multi-objective optimization of hybrid renewable energy systems with green hydrogen integration and hybrid storage strategies, Int. J. Hydrogen Energy, 142, 1249–1271, https://doi.org/10.1016/j.ijhydene.2025.03.006, 2025.

Tofighi-Milani, M., Fattaheian-Dehkordi, S., and Lehtonen, M.: Electrolysers: A Review on Trends, Electrical Modeling, and Their Dynamic Responses, IEEE Access, 13, 39870–39885, https://doi.org/10.1109/ACCESS.2025.3546546, 2025.

Tomić, A. Z., Pivac, I., and Barbir, F.: A review of testing procedures for proton exchange membrane electrolyzer degradation, J. Power Soruces, 557, 232569, https://doi.org/10.1016/j.jpowsour.2022.232569, 2023.

Tully, Z., Starke, G., Johnson, K., and King, J.: An Investigation of Heuristic Control Strategies for Multi-Electrolyzer Wind-Hydrogen Systems Considering Degradation, in: 2023 IEEE Conference on Control Technology and Applications (CCTA), Bridgetown, Barbados, 16-18 August 2023, 817–822, 2023.

van Phan, L., Nguyen-Dinh, N. P., Nguyen, K. M., and Nguyen-Duc, T.: Advanced frequency control schemes and technical analysis for large-scale PEM and Alkaline electrolyzer plants in renewable-based power systems, Int. J. Hydrogen Energy, 89, 1354–1367, https://doi.org/10.1016/j.ijhydene.2024.09.360, 2024.

Windpark Rhede GmbH & Co. KG: The wind farm, https://windpark-rhede.de/, last access: 15 January 2026, 2025.

Xu, B., Oudalov, A., Ulbig, A., Andersson, G., and Kirschen, D. S.: Modeling of Lithium-Ion Battery Degradation for Cell Life Assessment, IEEE Trans. Smart Grid, 9, 1131–1140, https://doi.org/10.1109/TSG.2016.2578950, 2018.

Yodwong, B., Guilbert, D., Phattanasak, M., Kaewmanee, W., Hinaje, M., and Vitale, G.: Faraday's Efficiency Modeling of a Proton Exchange Membrane Electrolyzer Based on Experimental Data, Energies, 13, 4792, https://doi.org/10.3390/en13184792, 2020.

Zheng, Y., Huang, C., Tan, J., You, S., Zong, Y., and Træholt, C.: Off-grid wind/hydrogen systems with multi-electrolyzers: Optimized operational strategies, Energy Convers. Manage., 295, 117622, https://doi.org/10.1016/j.enconman.2023.117622, 2023.

Zheng, Y., You, S., Bindner, H. W., and Münster, M.: Incorporating optimal operation strategies into investment planning for wind/electrolyser system, CSEE JPES, 8, 347–359, https://doi.org/10.17775/CSEEJPES.2021.04240, 2022.

Zhou, Z., Zheng, M., Dong, B., and Li, J.: Cluster allocation strategy of multi-electrolyzers in wind-hydrogen system considering electrolyzer degradation under fluctuating operating conditions, Renew. Energy, 242, 122381, https://doi.org/10.1016/j.renene.2025.122381, 2025.